Precision Agriculture (2021) 22:1768–1802
https://doi.org/10.1007/s11119-021-09811-0

Optimization of multi-source UAV RS agro-monitoring schemes designed for field-scale crop phenotyping

Wanxue Zhu[1,2] · Zhigang Sun[1,2,3,4] · Yaohuan Huang[2,5] · Ting Yang[4] · Jing Li[1] · Kangying Zhu[1,2] · Junqiang Zhang[6,7] · Bin Yang[7] · Changxiu Shao[1] · Jinbang Peng[1,2] · Shiji Li[1,2] · Hualang Hu[8] · Xiaohan Liao[2,5,9,10]

Accepted: 21 April 2021 / Published online: 3 May 2021

Abstract
Unmanned aerial vehicle (UAV) system is an emerging remote sensing tool for profiling crop phenotypic characteristics, as it distinctly captures crop real-time information on field scales. For optimizing UAV agro-monitoring schemes, this study investigated the performance of single-source and multi-source UAV data on maize phenotyping (leaf area index, above-ground biomass, crop height, leaf chlorophyll concentration, and plant moisture content). Four UAV systems [i.e., hyperspectral, thermal, RGB, and Light Detection and Ranging (LiDAR)] were used to conduct flight missions above two long-term experimental fields involving multi-level treatments of fertilization and irrigation. For reducing the effects of algorithm characteristics on maize parameter estimation and ensuring the reliability of estimates, multi-variable linear regression, backpropagation neural network, random forest, and support vector machine were used for modeling. Highly correlated UAV variables were filtered, and optimal UAV inputs were determined using a recursive feature elimination procedure. Major conclusions are (1) for single-source UAV data, LiDAR and RGB texture were suitable for leaf area index, above-ground biomass, and crop height estimation; hyperspectral outperformed on leaf chlorophyll concentration estimation; thermal worked for plant moisture content estimation; (2) model performance was slightly boosted via the fusion of multi-source UAV datasets regarding leaf area index, above-ground biomass, and crop height estimation, while single-source thermal and hyperspectral data outperformed multi-source data for the estimation of plant moisture and leaf chlorophyll concentration, respectively; (3) the optimal UAV scheme for leaf area index, above-ground biomass, and crop height estimation was LiDAR + RGB + hyperspectral, while considering practical agro-applications, optical Structure from Motion + customer-defined multispectral system was recommended owing to its cost-effectiveness. This study contributes to the optimization of UAV agro-monitoring schemes designed for field-scale crop phenotyping and further extends the applications of UAV technologies in precision agriculture.

Keywords Unmanned aerial vehicle (UAV) · Multispectral · Hyperspectral · Thermal · LiDAR · Phenotyping

✉ Zhigang Sun
sun.zhigang@igsnrr.ac.cn

Extended author information available on the last page of the article

Introduction

Maize (*Zea mays* L.) is known as one of the most important crops around the world, which plays an essential role in feeding the population and providing raw material for manufacturing (Széles et al., 2012). According to FAOSTAT 2018, China accounted for 22.42% of the worldwide total maize production in 2018; for China in 2018, maize accounted for 42.04% of total cereal production. Crop phenotyping is a rapid process for profiling crop phenotypic characteristics including e.g., 3-dimensional (3D) structure information (e.g., crop height (CH), leaf area index (LAI), canopy volume), physiological traits (e.g., above-ground biomass (AGB), plant moisture content (W), and blade thickness), and biochemical parameters (e.g., leaf/canopy chlorophyll/nitrogen content/concentration (LCC/CCC, LNC/CNC)) (Hunt et al., 2018; Su et al., 2019). Some phenotypic parameters are strongly related to photosynthesis, respiration, and transpiration processes of crops. Field-scale maize phenotyping provides precise spatial variability and uncertainty of crop growth status, which is significant to the optimization of spatial agro-management with a view towards improving crop production.

Considering ecological benefits and the sustainable development of agroecosystem, non-destructive and cost-effective approaches for field-scale crop monitoring are priorities in the areas of modern precision agriculture. Satellite remote sensing (RS) has been broadly applied in agro-monitoring, but it is impacted greatly by the coarse spatial resolutions and mixed pixels, the cloudy and rainy weather conditions, and fixed and long revisiting periods (Verrelst et al., 2015; Xie et al., 2019). In recent years, the unmanned aerial vehicle (UAV) RS becomes an alternative to mitigate the aforementioned issues owing to its versatility and cost-benefits (Bendig et al., 2015; Wang et al., 2019a, b). As an emerging technology, UAV systems can distinctly capture crop information on field scales (~ 10^{-4}–10^{6} m^2) which is sharply extended from the traditional crop phenotyping scales (~ 10^{-6}–10^{0} m^2). Besides, remotely sensed crop information with specific spectral requirements (e.g., narrow or broad bands, specific wavelengths) is available via UAV observations, thus providing a potential to improve the estimation/retrieval accuracy of crop phenotypic traits.

UAV RS has been widely applied in the estimation of crop phenotypic parameters at the field level (Duan et al., 2014; Kanning et al., 2018). Optical (400–1000 nm, e.g., RGB, multispectral (MS), and hyperspectral (HS)) (Jay et al., 2018; Xu et al., 2019a, b), thermal (TM, 3–18 μm) (Berni et al., 2009; Maimaitijiang et al., 2020), and light detection and ranging (LiDAR) (Luo et al., 2019) are three popular UAV sensors for RS-based vegetation phenotyping (Weiss et al., 2020). However, as the RS information offered by various UAV systems is characterized by different traits, the selection of appropriate UAV sensors depends on the specific phenotypic parameters.

Optical cameras have access to capture spectral reflectance and textures of objects, and vegetation indices (VIs) can be further calculated using the reflectance of specific bands (Cao et al., 2020; Chianucci et al., 2016). This optical information has been successfully applied in crop phenotyping with satisfying accuracies, such as the estimation/retrieval of above-ground biomass (Bendig et al., 2015), yield (Feng et al., 2020; Zhou et al., 2017), LAI (Roth et al., 2018), and LCC/CCC/LNC/CNC (Li et al., 2019; Zhu et al., 2020). However, the asymptotic saturation issue that occurred in the dense canopy would hamper the applications of optical sensors regarding crop phenotyping, independent and complementary RS information (e.g., temperature and vertical structure data of canopies) is therefore necessary to alleviate these issues.

In recent years, the structure from motion (SfM) point clouds has become a promising alternative for partially detecting canopy structure information (González-Jaramillo et al., 2019). SfM point cloud is developed from the image sequences caused by multi-angle tilt photogrammetry of optical cameras (usually are RGB and MS) (Li et al., 2016; Ye et al., 2019). However, these passive optical cameras fail to penetrate the dense canopy and capture precise information beneath the layers. Therefore, optical SfM point clouds are limited in detecting rugged terrain and complex vertical structure of canopies, especially for the forest ecosystem with abundant species diversity (Karpina et al., 2016). As farmland is usually under unified tillage management, crop canopy tends to be homogeneous. In such a context, the performance of optical SfM point clouds on revealing the subtle differences of a homogeneous crop canopy remains uncertain (Zhu et al., 2019a, b). By comparison, the LiDAR system, as an active technology, allows more dense point clouds concerning 3D information of observed objects from differences in the wavelengths and return time of the actively emitted laser (Luo et al., 2019). While it is challenging to apply LiDAR in agro-applications due to the over-expensiveness.

Temporal and spatial variations of soil moisture have important impacts on crop growth, but it is difficult to obtain these variations. Diagnosis of plants to indirectly assess environmental water stress has been proposed as an alternative approach in previous studies (Kullberg et al., 2017). Although VIs and fractional vegetation cover from optical data have the capabilities of assessing water stress severity for plants, the independent temperature information of canopies provided by TM cameras is the best indicator (Maes & Steppe, 2012). For example, the water stress level for crops can be assessed through the comparison between the target and fully irrigated reference crops; some TM related indicators, such as crop water stress index and canopy temperature ratio, have been generated to assess soil moisture deficit and related stress factors (Maimaitijiang et al., 2020; Taghvacian et al., 2012). The integration of TM into spectral and structure RS data can provide independent and complementary information for crop phenotyping, which could contribute to accurate estimation.

In this study, five key crop parameters, i.e., LAI, AGB, LCC, CH, and W were selected for UAV RS-based phenotyping, and the related studies were summarized in Table 1. Single and dual UAV sensors have been widely applied in the estimation of these five parameters. Concerning LCC estimation, optical, particularly HS sensors are broadly used (Jay et al., 2018; Zhu et al., 2020); LAI estimation is often carried out using the integration of 3D point clouds and optical information (Córcoles et al., 2013; Duan et al., 2014; Yang et al., 2017); for CH, 3D point clouds are often recommended (Niu et al., 2019); regarding AGB estimation, the fusion of optical information and 3D point clouds is popular (Almeida et al., 2019; Bendig et al., 2015); and the TM camera is usually targeted applied in the diagnosis of water stress levels or plant moisture content, since the TM bands are sensitive to water/moisture (Maes & Steppe, 2012). However, there is a scarcity of study that has integrated optical, LiDAR, and TM sensors together or intercompared the performances of multi-source UAV sensors for crop phenotyping. As appropriate combinations of UAV sensors contribute to accurate phenotyping, it is necessary to investigate the performance of single and multi-source UAV data in field-scale crop phenotyping.

This study aimed to fill a gap regarding field-scale crop phenotyping using multi-source UAV RS technologies and design optimal UAV agro-monitoring schemes. The hypotheses are that UAV 3D-related information performs well in LAI and CH estimation; spectral and thermal data are suitable for LCC and W estimation, respectively; and the fusion of multi-source UAV data contributes to crop phenotypic parameter estimation, especially for AGB. To test these hypotheses, simultaneous multi-source UAV data that were captured

Table 1 Summary of crop phenotyping using multi-source UAV RS technology

Phenotypic parameters	Commonly-used UAV sensors	References
LCC/CCC/LNC/CNC	1. MS	(Jay et al., 2018; Roosjen et al., 2018)
	2. HS	(Li et al., 2019)
LAI	1. RGB	(Córcoles et al., 2013)
	2. MS	(Jay et al., 2018; Yao et al., 2017)
	3. HS	(Duan et al., 2014)
	4. LiDAR	(Yang et al., 2017)
	5. RGB + MS	(Su et al., 2019; Yue et al., 2018)
	6. HS + MS	(Zhu et al., 2019a, b)
W/WSL[a]	1. TM	(Berni et al., 2009)
CH	1. SfM	(Li et al., 2016; Niu et al., 2019; Su et al., 2019)
AGB/yield	1. RGB/RGB + SfM	(Bendig et al., 2014; Niu et al., 2019)
	2. MS/MS + SfM	(Bendig et al., 2015; Roosjen et al., 2018; Wang et al., 2019a, b)
	3. HS/HS + SfM	(Yue et al., 2017)
	4. LiDAR	(Zhu et al., 2019a, b)
	5. MS + TM	(Maimaitijiang et al., 2020)

[a]*WSL* water stress level

via UAV RGB, HS, TM, and LiDAR systems were used for field-level estimation of maize phenotypic parameters (i.e., AGB, LAI, W, CH, and LCC). Pearson correlation analysis was used to filter highly correlated UAV inputs, and recursive feature elimination (RFE) feature selection was carried out to carefully select appropriate UAV inputs for models. Four statistical models, i.e., multi-variable linear regression (LM), backpropagation neural network (BP), random forest (RF) model, and support vector machine (SVM) were applied to modeling. Multiple models for parameter estimation aimed to mitigate the uncertainty of algorithms so as to ensure the reliability of phenotypic estimates. The results of this study would contribute to field-scale crop phenotyping based on UAV RS technologies and extend the applications of UAVs in precision and sustainable agriculture.

Material

Study area

The study site was set up at the Yucheng Comprehensive Experiment Station (YCES) of the Chinese Academy of Sciences, Dezhou city in the western Shandong Province in China (36.83° N, 116.57° E, Fig. 1). The study area is located at a temperate monsoon zone, with a mean annual rainfall of 582.0 mm/year and an average air temperature of 13.10 °C. Most of the precipitation is during the growth period of the maize. Wheat and maize are the dominant crops, which are cultivated between October and June in the following year, and between July and September, respectively.

Two long-term experimental fields in use over ten years were utilized for UAV and field observations. Field YF has 25 plots (5 × 6 m), applied with six fertilization and tillage

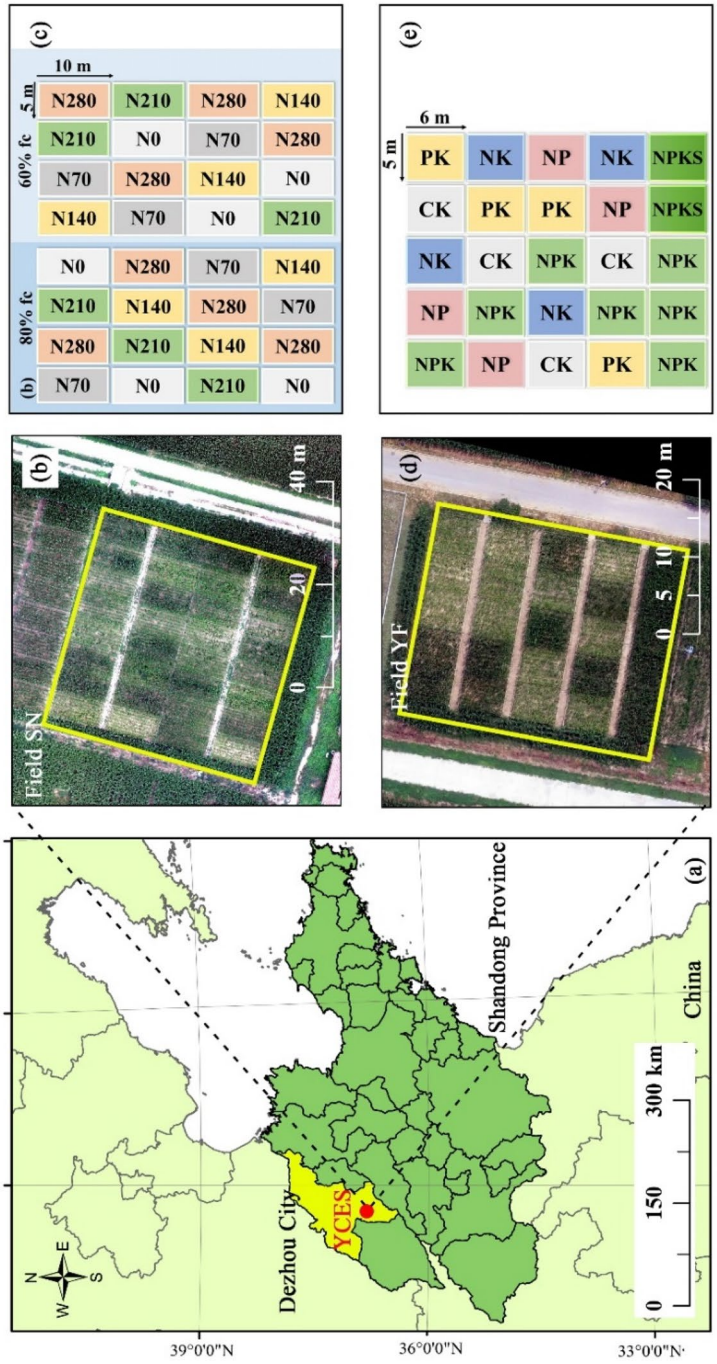

Fig. 1 **a** Geographic location of the study area (YCES); **b** overview of Field SN; **c** nitrogen fertilization and irrigation treatments for Field SN; **d** overview of Field YF; **e** nutrient and tillage treatments for Field YF

treatments: CK, NP, NK, PK, NPK, and NPKS; where N, P, K are nitrogen (N 255 kg ha^{-1}), potash (K_2O 125 kg ha^{-1}), and phosphate (P_2O_5 30 kg ha^{-1}) fertilizers, respectively; S is returning the whole straw of each plot into the soil; CK is no nutrient fertilizer. Because the bottom row of plots was used as reserved fields, these five plots were treated with conventional fertilization (two NPKS and three NPK plots). Field SN has 32 plots, with a size of 5 × 10 m. It was applied with two irrigation (60% fc, 80% fc) and five nitrogen fertilizer levels (N0, N70, N140, N210, and N280 denote 0, 70, 140, 210, and 280 kg N ha^{-1} for each crop season, respectively). The 60% fc and 80% fc denote irrigation to 60% and 80% of the field water capacity, respectively. Maize was irrigated once at the sowing stage.

Data acquisition

Field data collection

Summer maize (*Zea mays* L.), "Zhengdan 958", was planted on June 12, 2018, and June 15, 2018, for Fields YF and SN, respectively. Five crop phenotypic parameters were measured in this study, including LAI (m^2 m^{-2}), CH (cm), AGB (t ha^{-1}), W (%), and LCC (mg kg^{-1}) (Table 2). All the five parameters were measured on 22–24 July 2018 (Fig. 2). Crop canopies were homogeneous within a plot because of the scientific agro-management, while they were heterogeneous between various plots owing to the different tillage treatments. For ensuring the typicality of field sampling, considering the plot size, five plants outside the border area were determined on a random basis for field measurement.

Measurement of LCC and LAI were carried out in the field. LCC was non-destructively measured using a MultispecQ v2.0 handheld chlorophyll meter (PhotosynQ LLC, East Lansing, MI, USA), between 10:00 and 14:00 under a clear sky. MultispecQ v2.0

Table 2 Descriptive statistics for the five field-measured maize phenotypic parameters

Maize parameters	Field	Min	Mean	Max	SD[a]	cv (%)[b]
LAI (m^2 m^{-2})	Field all (n = 57)	0.35	1.17	2.36	0.47	39.87
	Field YF (n = 25)	0.50	1.37	2.36	0.58	42.29
	Field SN (n = 32)	0.35	1.00	1.48	0.26	25.73
AGB (t ha^{-1})	Field all (n = 57)	0.20	1.14	4.54	1.01	88.12
	Field YF (n = 25)	0.35	1.82	4.54	1.19	65.40
	Field SN (n = 32)	0.20	0.61	1.26	0.25	40.56
W (%)	Field all (n = 57)	84.35	87.57	89.13	1.17	1.34
	Field YF (n = 25)	84.35	86.81	89.01	1.28	1.47
	Field SN (n = 32)	86.52	88.16	89.13	0.62	0.71
LCC (mg kg^{-1})	Field all (n = 57)	26.72	37.21	50.26	4.25	11.43
	Field YF (n = 25)	26.72	39.33	50.26	4.40	11.18
	Field SN (n = 32)	27.93	35.56	41.00	3.36	9.46
CH (cm)	Field all (n = 57)	67.67	107.76	166.50	23.32	21.64
	Field YF (n = 25)	69.00	120.86	166.50	27.51	22.76
	Field SN (n = 32)	67.67	97.53	116.67	12.25	12.56

[a]*SD* standard deviation

[b]*cv* coefficient of variation

Fig. 2 **a** Destructive sampling of maize; **b** measurement of LCC using a MultispecQ; and **c** removing moisture of maize samples using an oven

was controlled by a Photosynq app through Bluetooth using an Android smartphone MI 8 (Xiaomi Technology Co., Ltd., Beijing, China). All the leaves of maize were used for LCC measurement, and each leaf was measured 3 times. MultispecQ v2.0 measurement recorded relative amounts of chlorophyll in leaves, this measurement gave a unitless but highly reproducible measure. The MultispecQ-based LCC (unitless) was further converted into actual LCC (mg kg^{-1}) based on the results of the previous study (Zhu et al., 2020). LAI was measured by a LAI-2200 Canopy Analyzer (Li-COR Biosciences, Lincoln, NE, USA), repeating 10 times in each plot. LAI measurement was conducted at dusk to avoid intense incident radiation.

The whole plant without roots was cut down for indoor measurement of AGB, CH, and W. Maize plant was put vertically to measure CH using a straight tape, measuring from the ground to the top part of the plant. Then the whole plants were used for weighing the fresh AGB (with moisture). Next, to remove moisture, maize was cut up and put into envelopes. The samples were dried in an oven at 105 °C for 2 h to destroy the activity of the enzyme and then at 75 °C until the weight remained constant to obtain the dry AGB (without moisture) and W. Field-level LAI, CH, and LCC were obtained by calculating the average values of all measurements; AGB and W of each plot were calculated as follows:

$$\mathrm{AGB}\left(\mathrm{kg\ m^{-2}}\right) = (m \times \mathrm{num})/(\mathrm{length\_plot} \times \mathrm{width\_plot}) \tag{1}$$

$$\mathrm{W}\ (\%) = (\mathrm{fresh\ AGB} - \mathrm{dry\ AGB})/(\mathrm{fresh\ AGB}) \times 100\% \tag{2}$$

$$\mathrm{Actual\ LCC}\left(\mathrm{mg\ kg^{-1}}\right) = 9.6324 \times e^{0.029 \times \mathrm{MultispecQ\ -\ based\ LCC}} \tag{3}$$

where m (kg) is the total weight of dry matter per maize plant; num is the number of plants in each plot; length_plot and width_plot are the length (m) and width (m) of each plot, respectively. Then the kg m^{-2} was rescaled to t ha^{-1}.

Multi-sensor UAV flights

Four UAV flight missions were conducted under clear sky and low wind speed (< 5 m s^{-1}) conditions between 09:30–14:30 Beijing time, on 22–24 July 2018, when the time at the jointing stage of maize. Four types of UAV platforms, i.e., eBee wing-fixed UAV (SenseFly, Cheseaux-Lausanne, Switzerland), DJI M100 four-rotator UAV (SZ DJI Technology

Co., Shenzhen, China), DJI M600 six-rotator UAV (SZ DJI Technology Co., Shenzhen, China), and EWZ-D6 six-rotator UAV (EWATT, Wuhan, China), were equipped with thermoMAP camera (SenseFly, Cheseaux-Lausanne, Switzerland), DJI Zenmuse X3 RGB camera (SZ DJI Technology Co., Shenzhen, China), Nano-Hyperspec VNIR HS camera (Headwall Photonics, Los Angeles, CA, USA), and the Alpha Series AL3-32 LiDAR system (Phoenix, Los Angeles, CA, USA), respectively (Fig. 3). The specific information about UAV systems and their flight missions is shown in Table 3.

For the next radiation calibration, the reflectance of spectral panels was collected before the flight of the RGB system and during the flight of the HS system. The calibration of TM data is automatic without artificial calibration. The Pix4D Mapper 3.1.22 (Pix4D, S.A., Lausanne, Switzerland) was used for the radiation correlation, image mosaic, and orthography of both RGB and TM images. The CloudCompare open-source software and ArcGIS 10.5 (ESRI, RedLands, CA, USA) were used for developing the digital surface model (DSM) and digital elevation model (DEM) derived from the LiDAR point clouds. ENVI 5.5 (Exelis Visual Information Solutions, Boulder, CO, USA) and IDL language were used for image mosaic and radiation correction of HS images. Python 3.7 and related geography processing packages (e.g., GDAL) were used for further processing and analysis of UAV RS data.

Methods

UAV RS information extraction

Extraction of hyperspectral information

The 272 raw HS bands (400–1000 nm) from Nano-Hyperspec VNIR HS orthomosaics were used as canopy spectral features. Besides, a set of VIs that have been applied to vegetation phenotyping recorded in previous studies was selected for parameter estimation. As shown in Table 4, these VIs were divided into five types: (1) $(R_1 - R_2)/(R_1 + R_2)$, (2) R_1/R_2, (3) $R_1 - R_2$, (4) $(R_1 - R_2)/R_3$, and (5) hybrid. The mean values of 272 bands and 27 VIs of each plot were calculated to present the spectral information of each plot. Thus, 272 spectral reflectance and 27 VIs constituted the HS dataset ($n = 299$).

Extraction of RGB information

As spectral information has been provided by HS camera, the RGB data with a high spatial resolution (~1 cm) were used to offer spectral texture information of canopies. This texture information was extracted from the grey level co-occurrence matrix (GLCM) of RGB-based green, red, and blue bands. GLCM texture includes eight indicators: mean, variance (var), homogeneity (homo), contrast (con), dissimilarity (dis), entropy (en), second moment (se), and correlation (cor). GLCM texture was computed using ENVI 5.5. The processing window is 3 rows × 3 cols. To obtain more texture information, the mean, min, max, sd, and cv values of GLCM indicators within each plot were calculated. Thus, 8 (GLCM indicators) × 3 (bands) × 5 (statistical metrics) = 120 RGB variables were generated for the RGB dataset.

Fig. 3 **a** DJI M600 and Nano-Hyperspec VNIR HS camera; **b** DJI M100 and DJI Zenmuse X3 RGB camera (in white, left); **c** eBee UAV and thermoMAP camera; and **d** EWZ-D6 and Alpha Series AL3-32 LiDAR system

Table 3 Specific information about four UAV systems and corresponding flight missions

Platforms	Sensors	
	Type	Specific information
eBee	ThermoMAP	(1) Bands: 3.5–13.5 µm (2) Scene temperature: − 40 ℃ to 160 ℃ (3) Temperature resolution: 0.1 ℃ (4) Calibration: automatic, in-flight thermal image-based (5) Spatial resolution: ~ 20 cm (6) Flight height: 105 m (7) Overlap: 70% (front), 80% (side)
DJI M100	DJI Zenmuse X3 RGB	(1) Bands: blue (B), green (G), and red (R) bands (2) Spatial resolution: ~ 1 cm (3) Flight height: 30 m (4) Overlap: 75% (front), 85% (side)
DJI M600	Nano-Hyperspec VNIR	(1) Bands: 400–1000 nm (272 bands) (2) Spectral resolution: ~ 2.22 nm (3) Spatial resolution: ~ 4 cm (4) Flight height: 60 m (5) 70% (front), 80% (side)
EWZ-D6	Alpha Series AL3-32 LiDAR	(1) Field View: 270° (2) Scan rate: 700 k points s^{-1} (3) Flight height: 40 m (4) Overlap: 70% (front), 70% (side)

Extraction of LiDAR information

The Alpha Series AL3-32 LiDAR system captured 3D point clouds of objects. Noise points were firstly filtered. Then DSM (raster data) was developed based on the remaining point clouds. Next, ground points were carefully selected to develop DEM. Thus CSM was available by the difference between DSM and DEM. The spatial resolution of DSM, DEM, and CSM were 2 cm × 2 cm. The mean, min, max, sd, and cv values of all CSM pixels within a plot were calculated. To obtain more LiDAR information, the GLCM approach was used again to obtain LiDAR-based canopy texture information. The process of LiDAR texture was similar to that of RGB data, including eight GLCM indicators, and each GLCM indicator had five statistical metrics. Thus, the LiDAR dataset was developed with $5 + 8 \times 5 = 45$ variables.

Extraction of thermal information

The temperature pixels of the maize canopy were captured by the thermoMAP camera. The min, mean, max, sd, cv, T05, T10, T15, T20, T25,T30, T35, and T40 values of each plot were calculated; where T05 T10, T15, T20, T25,T30, T35, and T40 were the mean values of top 5%, 10%, 15%, 20%, 25%, 30%, 35%, and 40% ranked pixels within a plot. The TM dataset was generated with 13 variables.

Table 4 Vegetation indices selected for crop phenotyping in this study

Name	Formulas	References
Formula form 1: $(R_1 - R_2)/(R_1 + R_2)$		
Normalized difference vegetation index 1	$NDVI1 = (R_{800} - R_{680})/(R_{800} + R_{680})$	(Yu et al., 2014)
Normalized difference vegetation index 2	$NDVI2 = (R_{531} - R_{570})/(R_{531} + R_{570})$	
Red edge NDVI 1	$NDRE1 = (R_{750} - R_{705})/(R_{750} + R_{705})$	
Red edge NDVI 2	$NDRE2 = (R_{790} - R_{720})/(R_{790} + R_{720})$	(Xie et al., 2019)
Normalized difference medium resolution imaging spectrometer vegetation index	$MERISND = (R_{754} - R_{709})/(R_{754} + R_{709})$	(Croft et al., 2020)
Green NDVI	$GNDVI = (R_{801} - R_{550})/(R_{801} + R_{550})$	(Daughtry et al., 2000)
Formula form 2: R_1/R_2		
Simple ratio	$SR = R_{800}/R_{550}$	(Daughtry et al., 2000)
Red edge reflectance ratio (710 nm)	$PR710 = R_{750}/R_{710}$	(Yu et al., 2014)
Red edge reflectance ratio (720 nm)	$PR720 = R_{740}/R_{720}$	
Pigment specific simple ratio	$PSSRa = R_{800}/R_{680}$	
Simple ration medium resolution imaging spectrometer vegetation index	$MERISSR = R_{754}/R_{709}$	(Croft et al., 2020)
Formula form 3: $R_1 - R_2$		
Reflectance difference 1	$RD1 = R_{800} - R_{680}$	(Yu et al., 2014)
Reflectance difference 2	$RD2 = R_{705} - R_{505}$	
Formula form 4: $(R_1 - R_2)/R_3$		
Plant senescence reflectance index	$PSRI = (R_{680} - R_{500})/R_{750}$	
Chlorophyll index red edge	$CI_{red\ edge} = (R_{750} - R_{700})/R_{700}$	
Chlorophyll index green	$CI_{green} = (R_{750} - R_{550})/R_{550}$	
Red edge (705 nm) relative indices	$RERI705 = (R_{705} - R_{665})/R_{865}$	(Xu et al., 2019a, b)
Red edge (783 nm) relative indices	$RERI783 = (R_{783} - R_{705})/R_{865}$	
Formula form 5: Hybrid		
Transformed chlorophyll absorption in reflectance index	$TCARI = 3[(R_{705} - R_{665}) - 0.2(R_{705} - R_{560})(R_{705}/R_{665})]$	(Haboudane et al., 2002)
Optimized soil adjusted vegetation index 1	$OSAVI1 = 1.16(R_{865} - R_{665})/(R_{865} + R_{665} + 0.16)$	(Xu et al., 2019a, b)

Table 4 (continued)

Name	Formulas	References
Enhanced vegetation index	$EVI = 2.5\ ((R_{nir} - R_r)/(R_{nir} + 6R_r - 7.5R_b + 1))$	(Peng et al., 2017)
Improved chlorophyll absorption ratio index	$MCARI = [(R_{700} - R_{670}) - 0.2(R_{700} - R_{550})(R_{700}/R_{670})]$	(Daughtry et al., 2000)
Soil adjusted vegetation index	$SAVI = (1 + 0.5)((R_{801} - R_{670})/(R_{801} + R_{670} + 0.5))$	
Optimized soil adjusted vegetation index 2	$OSAVI2 = 1.16((R_{800} - R_{670})/(R_{800} + R_{670} + 0.16))$	(Haboudane et al., 2002)
Red-edge vegetation stress index	$RVSI = [(R_{714} + R_{749})/2] - R_{735}$	(Almeida et al., 2019)
Modified simple ratio	$MSR = \left(R_{800}/R_{670} - 1\right)/\sqrt{R_{800}/R_{670} - 1}$	(Xie et al., 2019)
Modified simple ratio red edge	$MSRRE = (NIR/RE - 1)/\sqrt{NIR/RE - 1}$	(Dong et al., 2019)

Pre-process of 4 UAV datasets

As Fig. 4 shows, firstly, four UAV datasets (RGB, HS, LiDAR, and TM) were generated as foregoing descriptions (477 UAV variables). Secondly, the highly correlated UAV variables were removed ($|r| > 0.95$, $n = 57$) to reduce the impacts of the multi-collinearity issue (Almeida et al., 2019). This process was carried out using the *findCorrelation* function of the *caret* package in the R × 3.6.3 software. After this process, only 108 UAV variables remained. To select appropriate UAV variables for maize phenotyping and to ensure the accuracy of estimation models, the RFE feature selection was carried out using the *caret* package in R × 3.6.3. RFE feature selection is a wrapper method, which selects model inputs based on the value of root mean square error (RMSE) or the coefficient of determination (R^2). This process was quantified in three-fold cross-validation, repeating 1000 times. The optimal models were determined with the lowest RMSE. Finally, single-source and multi-source UAV datasets were separately used for modeling (see "Modeling and validation" section), and their performance was intercompared. Thus, optimal UAV observation schemes could be determined.

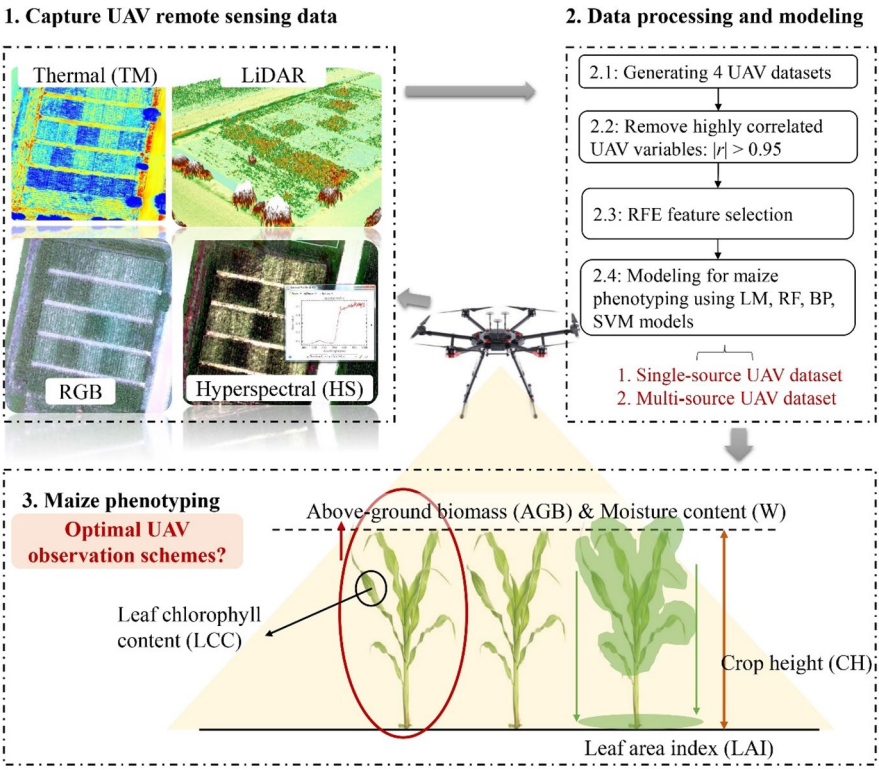

Fig. 4 A brief framework of maize phenotyping based on multi-source UAV data

Statistical analysis and methods used for phenotyping

Modeling and validation

Machine learning algorithms have been demonstrated to have the capability of conducting non-linear modeling flexibly with satisfying accuracy and robustness, and are adopted in data fusion-based estimation of crop phenotypic parameters (Cai et al., 2019). Factors such as the sample size, data characteristics, and initial parameterizations would affect model performance. To ensure the estimation reliability of UAV-based crop phenotyping, three machine learning methods (BP, RF, and SVM) and LM were used in this study, and their performance was intercompared. BP, RF, and SVM modeling were run using the *nnet*, *randomForest*, and *e1071* packages in R, respectively.

Machine learning modeling included three steps. Firstly, zero-mean normalization (z-score) and model parameterization were conducted. The z-score requires all UAV RS inputs were normalized to the mean and sd values of 0 and 1, respectively. The parameterization of the RF algorithm was the default value; the kernel of SVM was set to 'linear' mode; the *size*, *maxit*, and *decay* parameters of BP were debugged repeatedly to determine their optimal values for different phenotyping models. Secondly, the leave-one-out-cross validation (LOOCV) was carried out to avoid the multicollinearity issues by dividing the dataset into training ($n_{\text{train}} = 56$) and validation datasets ($n_{\text{vali}} = 1$). LOOCV is k-fold cross-validation, where k equals the number of samples ($k = n$). The LOOCV is time-consuming, but it is recommended for samples with a small size. As samples equal to 57, this process was repeated 57 times, and each model was repeated 1000 times. Finally, the performance of each model for maize phenotyping was assessed by the validation dataset, which was evaluated using R^2, RMSE, and the mean relative error (MRE) as follows:

$$R^2 = \frac{\sum_{i=1}^{n}\left(M_i - \overline{M}\right)\left(E_i - \overline{E}\right)}{\sqrt{\sum_{i=1}^{n}\left(M_i - \overline{M}\right)^2}\sqrt{\sum_{i=1}^{n}\left(E_i - \overline{E}\right)^2}}, \tag{4}$$

$$\text{RMSE} = \sqrt{\frac{\sum_{1}^{\text{n}}\left(M_i - E_i\right)^2}{\text{n}}}, \tag{5}$$

$$\text{MRE} = \frac{1}{\text{n}}\sum_{\text{i}=1}^{\text{n}}\frac{\left|M_i - E_i\right|}{M_i}, \tag{6}$$

ANOVA test

To further investigate the effects of tillage treatment of maize phenotypes, analysis of variability (ANOVA) was implemented for two fields. For Field YF, the six treatments (i.e., CK, NP, NK, PK, NPK, NPKS) were treated as a 'nutrient factor', so the one-way ANOVA test was implemented. The irrigation (fc) and nitrogen fertilizer (N) levels of Field SN were different, thus a two-factor interactive ANOVA test was conducted for Field SN. ANOVA

test was conducted using the IBM SPSS statistics 24.0 software (IBM Corp., Armonk, NY, US).

Results

Effects of tillage treatment on maize phenotyping

As shown in Fig. 5, in Field YF, LAI, AGB, CH, and LCC exhibited obvious spatial heterogeneity across various nutrient and tillage treatments, with a similar trend that their values roughly increased in the order of NPKS > NPK > NP > PK > NK > CK; while the variance of W across various plots was not remarkable, as the W values were 85.37 ± 0.92%, 86.30 ± 1.36%, 86.30 ± 0.73%, 86.47 ± 0.38%, 87.82 ± 0.70%, and 88.83 ± 0.25% for CK, NK, NP, PK, NPK, NPKS plots, respectively. In Field SN, LAI, AGB, CH, and LCC were approximately correlated with N fertilizer levels, although their values nearly remained constant when the plots were applied over a rate of 210 kg N ha^{-1}. However, the W values were 87.50 ± 0.70%, 88.45 ± 0.32%, 88.09 ± 0.76%, 88.31 ± 0.38%, and 88.40% ± 0.49 for N0, N70, N140, N210, and N280 plots, respectively. Besides, the W value of 80% fc plots (88.30 ± 0.69%) was close to that of 60% fc plots (88.03 ± 0.53%), suggesting the insignificant difference of plant moisture content for plots in Field SN; while regarding the other four phenotypic parameters, the growth of maize at 80% fc was better than 60% fc.

Differences in maize phenotypic parameters across various tillage treatments were assessed using the ANOVA test. The Psig. values for tillage factor on LAI, AGB, CH, LCC, and W at Field YF were less than 0.05 (F test, $n = 25$) (Table 5), suggesting the N, P, and K fertilizer along with straw returning treatments had major effects on maize phenotype. As shown in Table 6, The Psig. values for N fertilizer levels on LAI, AGB, CH, and LCC were < 0.05 ($n = 32$), indicating N levels had a significant impact on maize LAI, AGB, CH, and LCC. While, the irrigation levels only influenced AGB and CH significantly (Psig. < 0.05, $n = 32$). Except for W, no significant differences were found in LAI, AGB, CH, and LCC between the interactive treatments of N and irrigation within Field SN.

Maize phenotyping using single-source UAV RS data

Model inputs screening of single-source UAV data

This section used four single-source UAV datasets for maize phenotyping. The effects of UAV input sizes on phenotyping and the importance values of the top 10 ranked UAV variables were displayed in Figs. 6 and 7, respectively. When the RMSE was lowest, the number of inputs was determined as an optimal size. However, taking temporal efficiency, model robustness, and the importance of UAV inputs into account, the most parsimonious yet informative model was determined.

For LAI estimation, the optimal sizes of UAV inputs were 5, 21, 3, and 2 for LiDAR, HS, RGB, and TM datasets, respectively; the RMSE values were in the order of LiDAR (~ 0.20) < RGB (~ 0.30) < HS (~ 0.32) < TM (~ 0.35) (Fig. 6). Among LiDAR variables, Li-mean, Li-sd, and Li-cv were essential for modeling, as their importance values were 16.82, 15.82, and 15.51, respectively (Fig. 7). The importance of HS variables was close ranging between 4.70 and 7.84, and most of the top 10 ranked important variables were

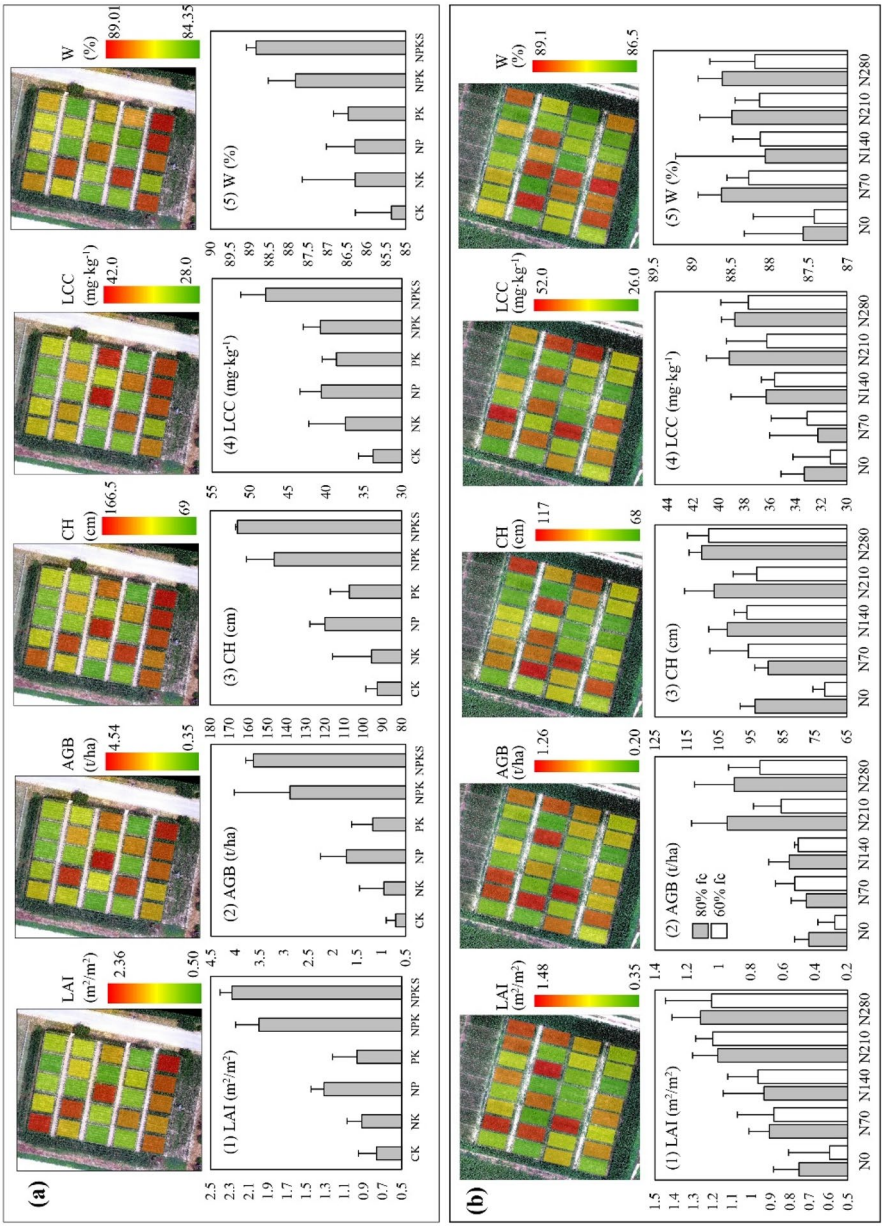

Fig. 5 Field measurements of phenotypic parameters of maize cultivated across various agronomic treatments: **a** Field YF and **b** Field SN

Table 5 Results of one-way ANOVA analysis for phenotypic parameters of maize at Field YF

		SS[a]	df	MS[b]	F	Psig		SS	df	MS	F	Psig
Groups	LAI	6.934	5	1.461	34.605	0.000	AGB	24.049	5	4.810	9.027	0.000
Error		1.374	19	0.042				10.123	19	0.533		
Total		8.309	24					34.172	24			
Groups	CH	15,070.046	5	3014.009	18.510	0.000	LCC	306.971	5	61.394	7.438	0.001
Error		3093.714	19	162.827				156.831	19	8.254		
Total		18,163.760	24					463.802	24			
Groups	W	26.228	5	5.246	7.618	0.000						
Error		13.083	19	0.689								
Total		39.310	24									

[a]*SS* sum of squares

[b]*MS* mean square

Table 6 Results of two-factor interactive ANOVA analysis for phenotypic parameters of maize at Field SN

	df	MS	F	Psig	df	MS	F	Psig	df	MS	F	Psig
	LAI				AGB				CH			
N	4	0.344	11.714	**0.000**	4	0.261	9.886	**0.000**	1	648.798	14.950	**0.000**
fc	1	0.010	0.355	0.558	1	0.131	4.984	**0.036**	4	436.219	10.051	**0.004**
N*fc	4	0.009	0.307	0.870	4	0.034	1.302	0.300	1	174.451	4.020	**0.014**
	LCC				W							
N	4	49.758	8.528	**0.000**	4	0.939	2.763	0.053				
fc	1	10.652	1.826	0.190	1	0.456	1.341	0.259				
N*fc	4	3.103	0.532	0.714	4	0.064	0.189	0.942				

The bold numbers aimed to highlight significance values were less than 0.05

red-edge and NIR bands, located at 730–750 nm and 930–980 nm, respectively. As the RMSE value of 6 HS variables (0.285) was roughly equivalent to 21 HS variables (0.274), the appropriate size of HS dataset for LAI estimation was set to 6. Among RGB variables, R-mean-mean was dominant for modeling (21.94) over the other variables. Regarding TM variables, T-max and T-min, and T-mean were important, with values of 22.12, 19.48, and 8.02, respectively.

In terms of AGB modeling, the optimal sizes of UAV inputs were 12, 12, 6, and 2 for LiDAR, HS, RGB, and TM datasets, respectively; while 5, 4, 6, and 2 were set as the appropriate size following the aforementioned rules. The RMSE were in the order of LiDAR (~0.52) < RGB (~0.62) < TM (~0.70)/HS (~0.70). The important LiDAR variables for AGB modeling were similar to LAI estimation, such as Li-mean (8.41), Li-sd (7.62), and Li-homo-mean (7.85). R-mean-mean was a dominant RGB variable with an importance value of 19.33, remarkably higher than the 2nd ranked G-mean-mean (9.29). Regarding HS variables, their importance values were low, most of which were located at NIR bands (930–960 nm). For TM dataset, the dominant variable was T-max, with an importance value of 28.72.

In the case of CH modeling, the appropriate size of UAV inputs were 7, 5, 3, and 2 for LiDAR, HS, RGB, and TM datasets, respectively. The RMSE values followed the

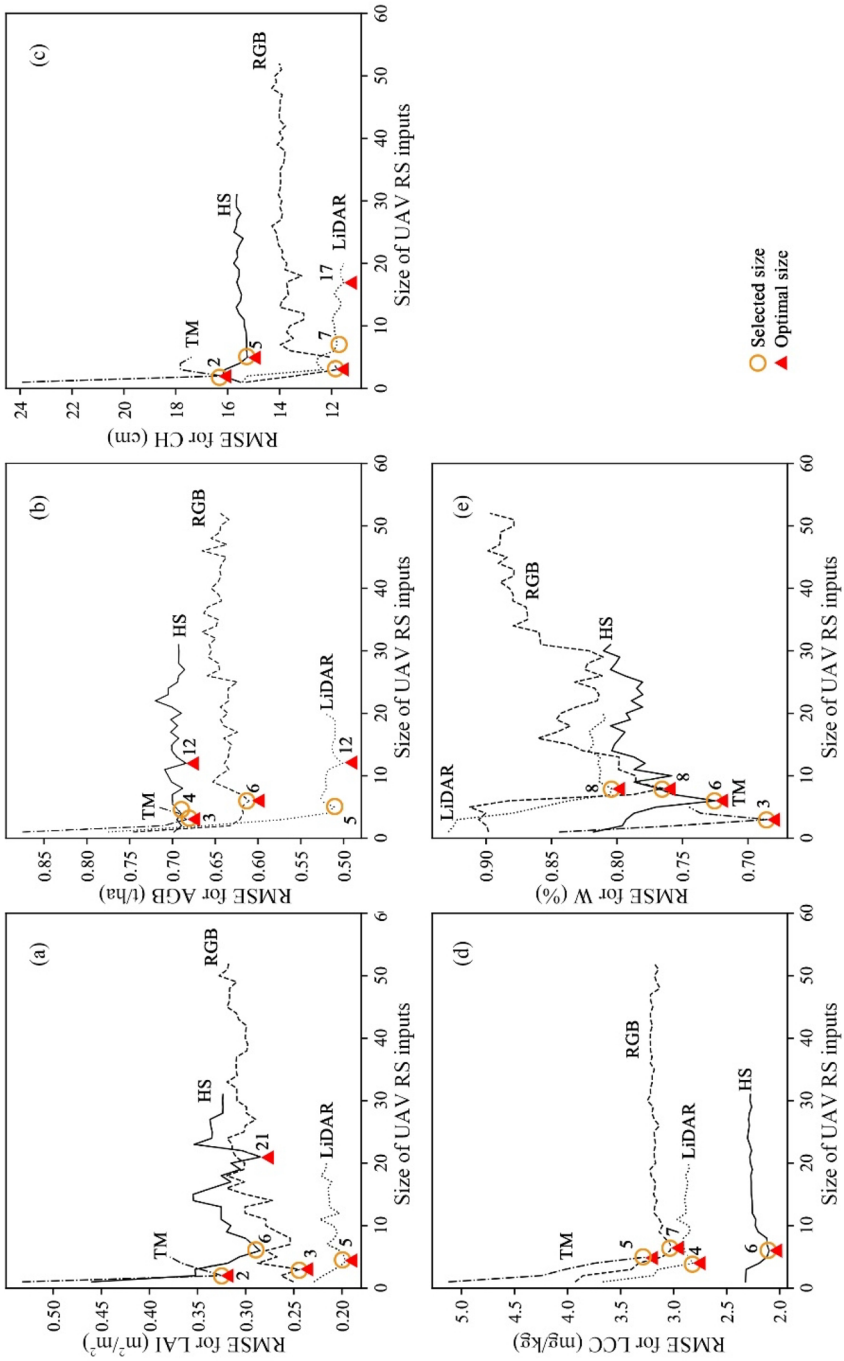

Fig. 6 The effects of UAV RS input sizes on the cross-validated RMSE of models for **a** LAI, **b** AGB, **c** CH, **d** LCC, and **e** W estimation

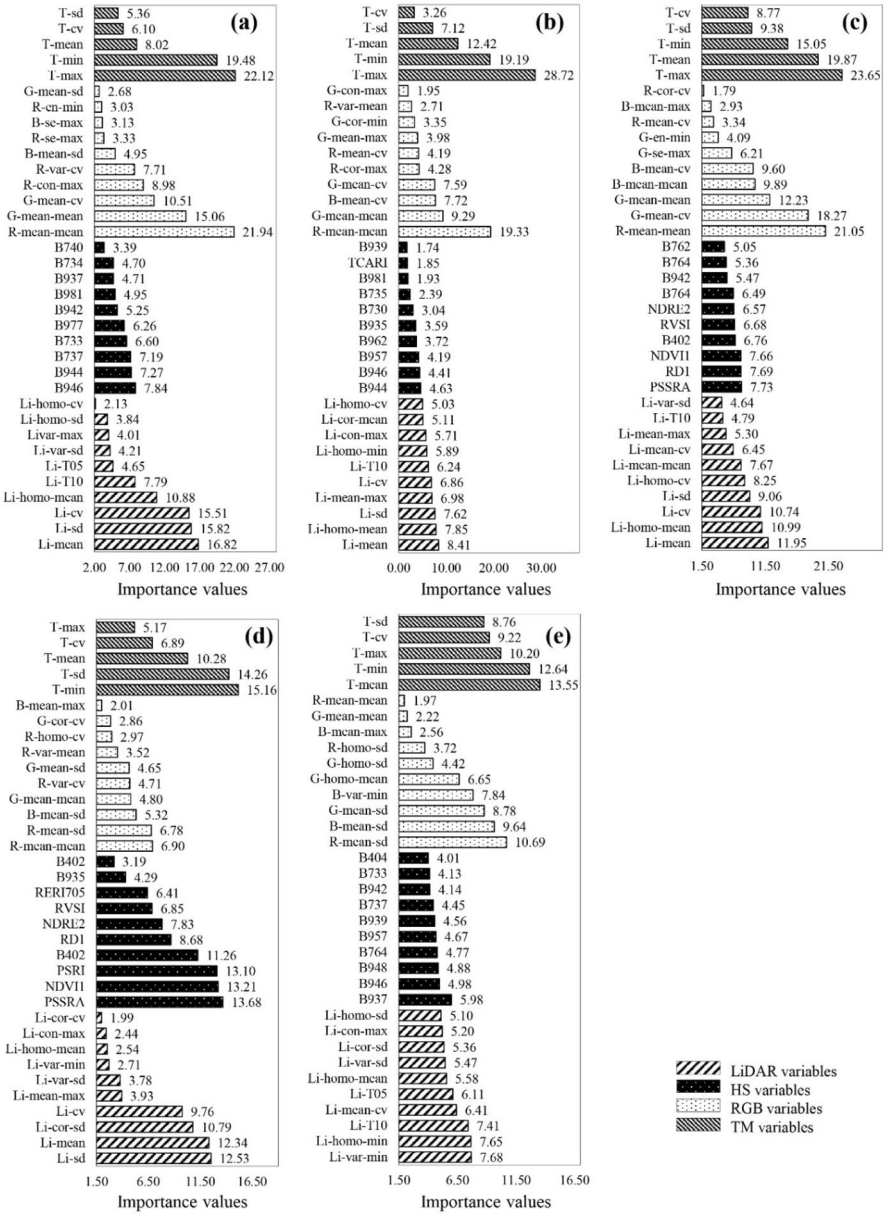

Fig. 7 Importance values for single-source UAV RS datasets on the cross-validated RMSE of models for **a** LAI, **b** AGB, **c** CH, **d** LCC, and **e** W estimation

order of LiDAR (~ 12.0) < RGB (~ 14.0) < HS (~ 15.30) < TM (~ 17.0). The important LiDAR, RGB, and TM variables were similar to AGB estimation. However, it is worth noting that the VIs (e.g., DR1, PSSRA, and NDVI1) were more important than the spectral reflectance of bands.

For LCC modeling, the appropriate sizes of UAV inputs were set to 4, 6, 7, and 5 for LiDAR, HS, RGB, and TM datasets, respectively. It should be noted that the HS dataset showed dominant advantages over LiDAR, TM, and RGB datasets, as the order of average RMSE was HS (~2.25) < LiDAR (~2.805) < TM/RGB (~3.20). The top six ranked important HS variables were PSSRA, NDVI1, PSRI, B402, RD1, and NDRE2, with corresponding importance values of 13.68, 13.21, 13.10, 11.26, 8.68, and 7.83, respectively.

As for W modeling, the appropriate sizes of LiDAR, HS, RGB, and TM datasets were set to 8, 6, 8, and 3, respectively. The RMSE values followed the order of TM (~0.73) < HS < (0.78) < LiDAR (~0.80) < RGB (~0.85), indicating that the TM dataset pertained to W estimation. The importance values of top 5 ranked TM-variables followed the order of T-mean (13.55) > T-min (12.64) > T-max (10.20) > T-cv (9.22) > T-sd (8.76).

Performance of single-source UAV data on maize phenotyping

After determining appropriate UAV variables, LM, RF, BP, and SVM methods were employed for maize phenotyping using single-source UAV data. The performance of various single-source UAV data on maize phenotyping was evidently different (Fig. 8). For LAI estimation, the accuracy of UAV datasets were in the order of LiDAR (R^2 = 0.83–0.85, RMSE = 0.18–0.19, MRE = 14.16–15.45%) > RGB (R^2 = 0.65–0.73, RMSE = 0.24–0.28, MRE = 16.98–20.52%) > HS (R^2 = 0.60–0.61, RMSE = 0.29–0.30, MRE = 21.19–24.70%) > TM (R^2 = 0.51–0.57, RMSE = 0.31–0.33, MRE = 23.83–26.80%). Regarding AGB estimation, the LiDAR dataset performed best, with R^2, RMSE, and MRE values around 0.70, 0.52, and 35%, respectively; the RGB dataset was less accurate than LiDAR dataset, while the performance of HS and TM datasets was comparable, remarkably less accurate than the LiDAR dataset. For CH estimation, the R^2, RMSE, and MRE values for LiDAR dataset were ranging 0.72–0.76, 11.49–13.58, and 9.13%–10.08%, respectively; and those three for RGB dataset were 0.63–0.69, 12.95–14.27, and 10.10–11.0%, respectively. The estimation for TM and HS datasets was less robust, with low R^2 and high RMSE and MRE. In terms of LCC, the HS dataset outperformed the other three datasets, with R^2, RMSE, and MRE around 0.76, 2.0, and 4.20%, respectively; while the RGB and TM datasets did not work well, with R^2, RMSE and MRE around 0.50, 3.2, and 6.0%, respectively. In the context of W estimation, the accuracy of UAV datasets were in the order of TM (R^2 = 0.65–0.69, RMSE = 0.69–0.71, MRE = 0.61–0.68%) > HS (R^2 = 0.59–0.63, RMSE = 0.71–0.75, MRE = 0.61–0.66%) > RGB (R^2 = 0.50–0.60, RMSE = 0.75–0.95, MRE = 0.72–0.77%)/LiDAR (R^2 = 0.55–0.56, RMSE = 0.77–0.80, MRE = 0.69–0.75%).

In summary, LiDAR and RGB datasets performed well in LAI, AGB, and CH estimation, although the LiDAR dataset was slightly better than the RGB dataset; HS outperformed the other three datasets in the case of LCC estimation; TM dataset did not perform well regarding maize phenotyping, although it moderately pertained to W estimation.

Maize phenotyping using multi-source UAV RS data

Model inputs screening of multi-source UAV data

In this selection, multi-source UAV data were used for maize phenotyping. As displayed in Fig. 9(1), models with the lowest RMSE values for LAI, AGB, CH, and W estimation required few UAV inputs, as their optimal feature sizes were 10, 11, 15, and 15, respectively. However, the optimal size for LCC modeling was 25. As the RMSE value of size

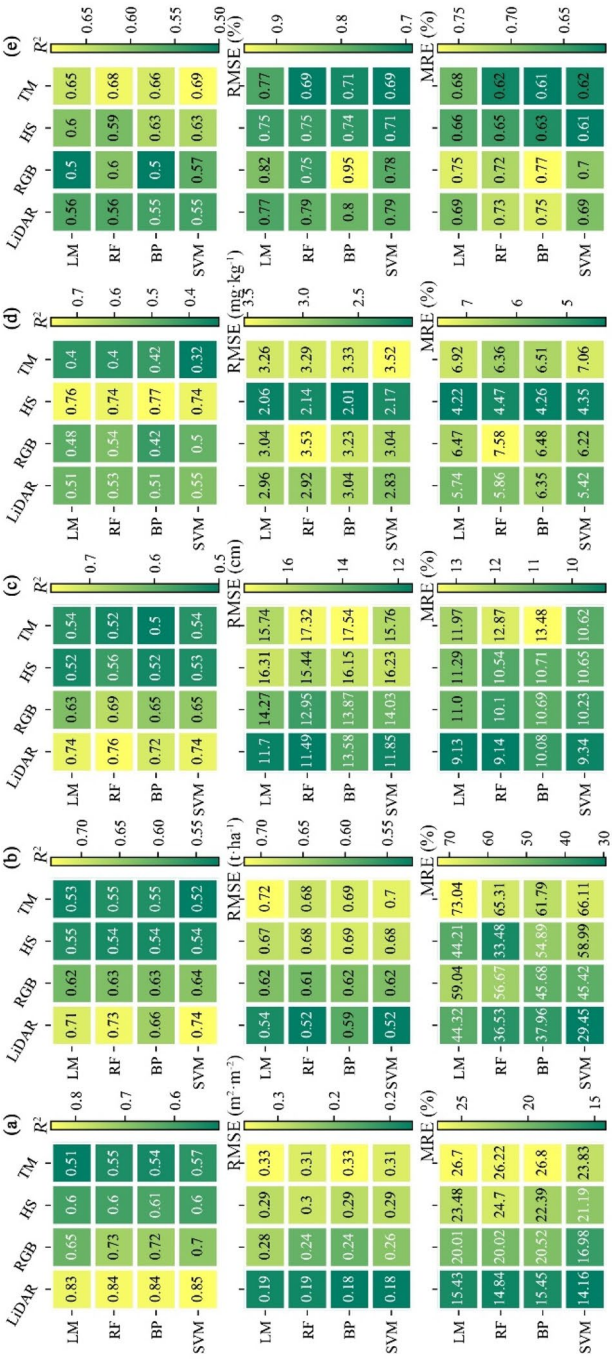

Fig. 8 R^2, RMSE, and MRE for linear regression between estimated and measured **a** LAI, **b** AGB, **c** CH, **d** LCC, and **e** W using single-source UAV RS data

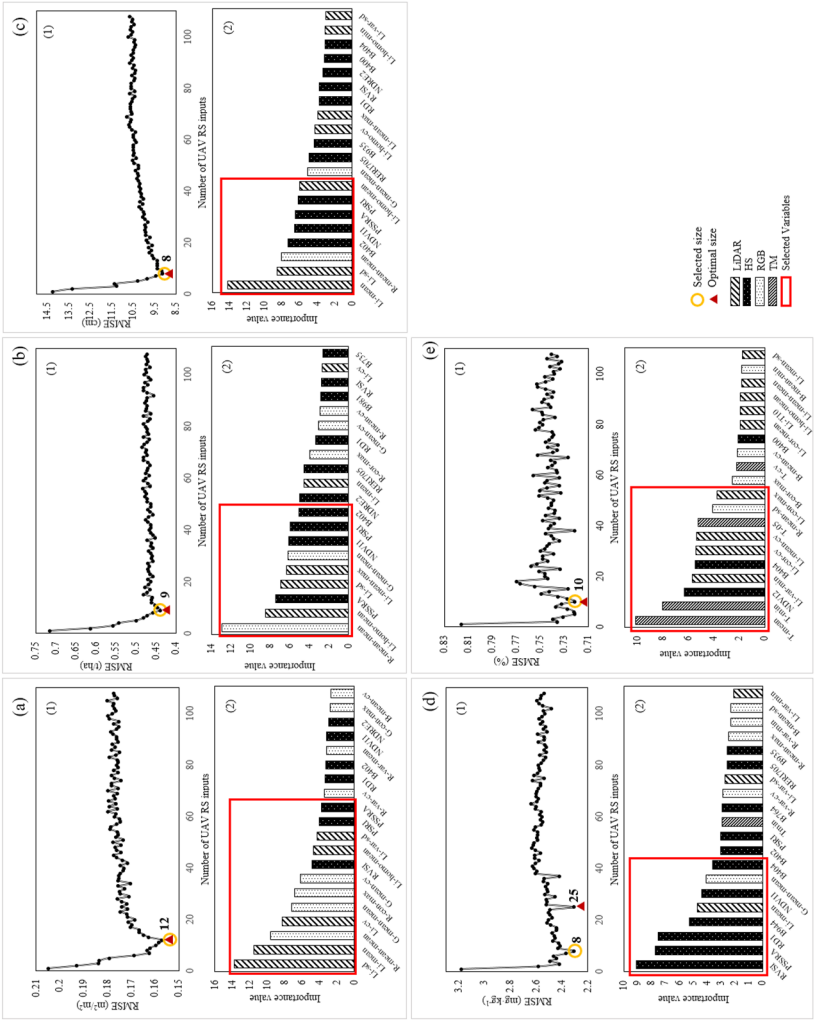

Fig. 9 Model inputs screening of multi-source UAV RS data: (1) the effect of feature size on the cross-validated RMSE of models; (2) the importance values for each UAV RS datasets for **a** LAI, **b** AGB, **c** CH, **d** LCC, and **e** W estimation

8 for LCC estimation was 0.809, close to size 83 (0.776), the appropriate size regarding LCC estimation was set to 8.

Comparing the importance values of multi-source UAV variables (Fig. 9(2)), for LAI estimation, the top 10 ranked UAV inputs, which would be used for the next LAI modeling, were Li-sd (13.82), Li-mean (11.03), R-mean-mean (9.75), Li-cv (8.11), R-con-max (7.07), G-mean-mean (6.83), RVSI (6.41), G-mean-cv (5.28), Li-homo-mean (4.47), and PSRI (4.18). Regarding CH modeling, Li-mean was dominant with an importance value of 14.06, followed by Li-sd (8.89), R-mean-mean (7.80), G-mean-mean (6.85), and PSSRA (6.72), et al. For AGB, four LiDAR, two RGB, and five HS variables were selected for modeling, suggesting comprehensive multi-source UAV RS information was needed for robust AGB estimation. Regarding LCC modeling, a LiDAR, three RGB, and 11 HS variables were listed in the selected model inputs, indicating HS dataset played the predominant role in LCC estimation. Besides, it should be noted that the top five ranked important variables were VIs in HS variables, i.e., PSRI (10.17), PSSRA (9.71), NDVI1 (9.31), RD1 (9.29), and B402 (8.13), indicating the performance of VIs was more stable and superior than band reflectance. TM dataset played a decisive role in W estimation, as the importance values of top two ranked UAV variables were 9.88 (T-min) and 9.45 (T-mean), remarkably higher than the following selected inputs e.g., Li-T10 (6.56), Li-mean-sd (6.55), and Li-mean-cv (5.76).

Performance of multi-source UAV data on maize phenotyping

Table 7 shows the robustness assessment of maize phenotyping using multi-source UAV RS data. Except for W, the estimation of LAI, AGB, CH, and LCC achieved satisfying accuracy. Regarding AGB estimation, the R^2 ranged between 0.79 and 0.81; RMSE ranged between 0.45 and 0.46; MRE ranged between 31.58 and 39.42%. While except for the BP performance was slightly poor, the R^2 values were around 0.88, 0.80, and 0.73, and RMSE values were around 0.16, 10.0, and 2.30 for LAI, CH, and LCC estimation, respectively. The estimation accuracy of W was moderate, with R^2, RMSE, and MRE around 0.60, 0.90, and 0.80%, respectively.

Table 7 R^2, RMSE, and MRE values for maize phenotyping using multi-source UAV data

	LAI (m^2 m^{-2})			AGB (t ha^{-1})			CH (cm)		
	R^2	RMSE	MRE	R^2	RMSE	MRE	R^2	RMSE	MRE
LM	0.86	0.20	17.34	0.79	0.45	31.58	0.80	10.96	8.68
RF	0.88	0.16	12.25	0.81	0.46	33.50	0.82	9.94	8.28
BP	0.84	0.19	14.08	0.79	0.46	39.42	0.76	12.00	10.36
SVM	0.89	0.16	13.24	0.80	0.46	34.57	0.79	10.54	7.89
	LCC (mg kg^{-1})			W (%)					
LM	0.72	2.29	5.18	0.59	0.94	0.90			
RF	0.74	2.31	5.31	0.65	0.74	0.68			
BP	0.66	2.69s	6.04	0.56	0.91	0.77			
SVM	0.73	2.47	5.47	0.61	0.73	0.65			

Discussion

In this study, five crop phenotypic parameters (i.e., LAI, AGB, CH, LCC, and W) were measured at the jointing period of maize cultivated across various tillage treatments, and the single-source and multi-source UAV RS datasets (i.e., HS, LiDAR, TM, and RGB) were used for maize phenotyping. The results of this study illustrated that for single-source UAV data, the LiDAR and RGB data were suitable for LAI, AGB, and CH estimation; HS data performed best regarding LCC estimation; while the TM dataset was appropriate for W estimation. The fusion of multi-source UAV RS data (LiDAR + RGB + HS) exhibited good performance regarding LAI, AGB, and CH estimation, although the importance of various UAV datasets differed for specific phenotypic parameters. While the single-source TM and HS data showed better performance than multi-source data on W and LCC estimation, respectively.

Selection of single-source UAV RS data for field-scale maize phenotyping

The results of this study validated that different-source UAV RS datasets were suitable for specific crop phenotypic parameters. To investigate the effects of relationships between crop parameters on UAV-based maize phenotyping, the Pearson correlation analysis was employed. For all samples ($n = 57$), CH, LAI, and AGB exhibited strongly linear relationship, as the r values were 0.84 for LAI and AGB ($p < 0.001$), 0.89 for LAI and CH ($p < 0.001$), and 0.93 for AGB and CH ($p < 0.001$). LCC also showed significant correlation with CH (0.82, $p < 0.001$), LAI (0.75, $p < 0.001$) and AGB (0.75, $p < 0.001$). However, W exhibited a weak correlation with LAI, LCC, AGB, and CH, with r values less than 0.27 ($p \geq 0.05$) (Fig. 10).

In this study, Li-mean was predominant on CH estimation, which is also recognized in previous studies that 3D point clouds and GLCM texture can provide information about canopy structure (Maimaitijiang et al., 2020; Schneider et al., 2019). As CH was illustrated to be strongly correlated to AGB and LAI, UAV-based LiDAR and GLCM texture information consequently would contribute to LAI and AGB estimation, which agrees with the previous studies (Li et al., 2016; Yue et al., 2017). However, the RGB and LiDAR data tend to suffer information overlap in the case of canopy structure detection, which might lead to the comparable applicability of LiDAR and RGB datasets. Nonetheless, RGB and LiDAR are independent, as RGB information was derived from optical photogrammetry while LiDAR data was extracted from 3D point clouds computed by active emitted laser. Besides, LiDAR outperformed RGB in LAI, AGB, and CH estimation, which is likely because the dense LiDAR scanning provided more precise structure information. On the other hand, RGB camera is a passive sensor and easily affected by environmental conditions (e.g., incident radiation, soil, weeds, and shadow), which might degrade its accuracy for remotely sensed observation.

In this study, the optical (MS/HS) dataset was proved to be appropriate for LCC estimation, which was consistent with the previous studies (Kanning et al., 2018; Pablo Rivera-Caicedo et al., 2017); while this single-source optical information exhibited moderate performance on LAI estimation. Many studies have validated that spectral information had the potential for LAI estimation, as they succeeded in implementing the spectral information and radiative transfer models (e.g., PROSAIL and ACRM) to retrieve LAI with a satisfying accuracy (Dong et al., 2019; Jay et al., 2017). The moderate performance of HS dataset

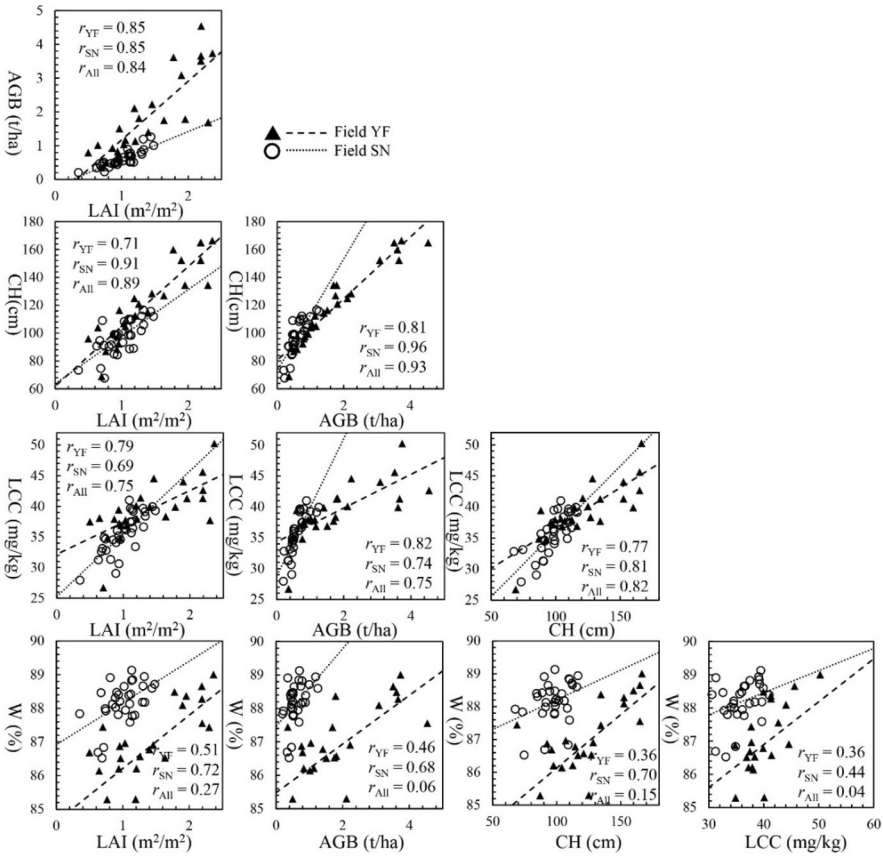

Fig. 10 Scatters of ground-measured phenotypic parameters of maize cultivated at Fields YF and SN

on LAI estimation could be explained by the asymptotic saturation that occurs for dense and heterogeneous canopies and surrounding noises within sparse canopies (Almeida et al., 2019; Gnyp et al., 2014). The tillage treatments of Fields SN and YF were different, and the sowing date of Field YF was three days earlier than Field SN. In such a context, the growth process of maize differed among various plots. Some maize without nutrient or irrigation stress, such as the NPKS plots in Field YF, were at the late jointing stage with relatively dense canopies; while maize under a severe environmental stress condition (e.g., N0 + 60%fc in Field SN) was at the early jointing stage with a sparse canopy. Consequently, part of plots with dense canopies might exhibit asymptotic saturation, while plots with sparse canopy might be obviously interfered with surrounding noises. As the variance of LAI across various tillage treatments was more obvious than LCC, the saturation issue could degrade LAI estimation more evidently compared to LCC estimation.

The temperature information provided by TM camera is associated with leaf water content, pigment content, and canopy structure features (Berni et al., 2009; Maimaitijiang et al., 2020). However, a wide range of environmental factors, for example, wind speed, photosynthetic active radiation, air temperature, and water availability, significantly affected canopy temperature, which may at least in part degrade TM performance

(Kullberg et al., 2017; Lei et al., 2020). Nonetheless, in this study, TM data was proved to exhibit potential in maize phenotyping, particularly for plant moisture content detection. Besides, since temperature data is independent and complementary to spectral and structure information, integration of these data for more robust crop monitoring and phenotyping is promising in recent years (Maimaitijiang et al., 2020).

Effects of multi-source data fusion on field-scale maize phenotyping

To investigate the effects of UAV data fusion on maize phenotyping, the differences in estimation robustness between multi-source and single-source datasets were displayed in Fig. 11. It should be noted that the accuracy improvement was not substantial when combing all spectral, structure, thermal, and texture information as compared to using optimal single-source UAV data, which is likely attributed to the information homogeneity and redundancy among canopy spectral, structure, and texture features.

The phenotyping results of data fusion illustrated that the combinations of LiDAR, RGB, and HS data exhibited slightly better performance on LAI, CH, and AGB estimation. This subtle improvement might be because the estimation accuracy of LiDAR-based model was already pretty high, and the errors and redundancy from surrounding noises offset the model improvement provided by the fusion of HS information. Nevertheless, AGB is a comprehensive parameter of crop growth status, which is strongly related to e.g., the accumulation of organic matters, the increase of CH and LAI, and changes in LCC (Xu et al., 2019a, b; Ye et al., 2020), thus AGB estimation required sufficiently independent and complementary RS data to ensure its comprehensiveness and robustness. In recent years, the fusion of LiDAR and HS data for AGB estimation is popular, particularly for forest ecosystems (Almeida et al., 2019; Luo et al., 2019). One reason could be that HS data has potential for species confirmation and assessment of vegetation physiological indicators, while LiDAR can mitigate the spectral asymptotic saturation, and offer supplementary information associated with canopy spatial heterogeneity and subtle structure characteristics.

The fusion of UAV datasets using four methods slightly degraded LCC and W estimation. In terms of LCC estimation, the R^2 decreased by 0.04, 0.01, and 0.11 for LM, SVM, and BP, respectively; the RMSE and MRE values of four methods were slightly increased. LCC is a biochemical indicator of vegetation, so few studies applied structural or temperature information to retrieve LCC. Besides, compared to spectral reflectance, VIs reduce the effects of environmental noises, and the implied information of crops could emerge through mathematics calculations and band combinations, so VIs are broadly used for vegetation phenotyping (Zhu et al., 2019a, b). Regarding W estimation, the accuracy nearly remained constant, without obvious change, although the performance of single-source TM dataset was slightly better than the multi-source UAV dataset. As demonstrated in Fig. 10, W showed a weak correlation with other parameters, so other UAV datasets that reflect e.g., spectral and structure information of canopies, might not offer effective information to boost the W estimation accuracy.

Effects of model construction on field-scale maize phenotyping

LM, RF, and SVM generally exhibited close performance in both single-source and multi-source estimation cases, which might be due to the limited samples and inputs for modeling. LM, RF, and SVM estimated LAI, AGB, CH, and LCC with satisfying accuracy, while the performance of BP was slightly unstable. As reported in previous studies, BP is

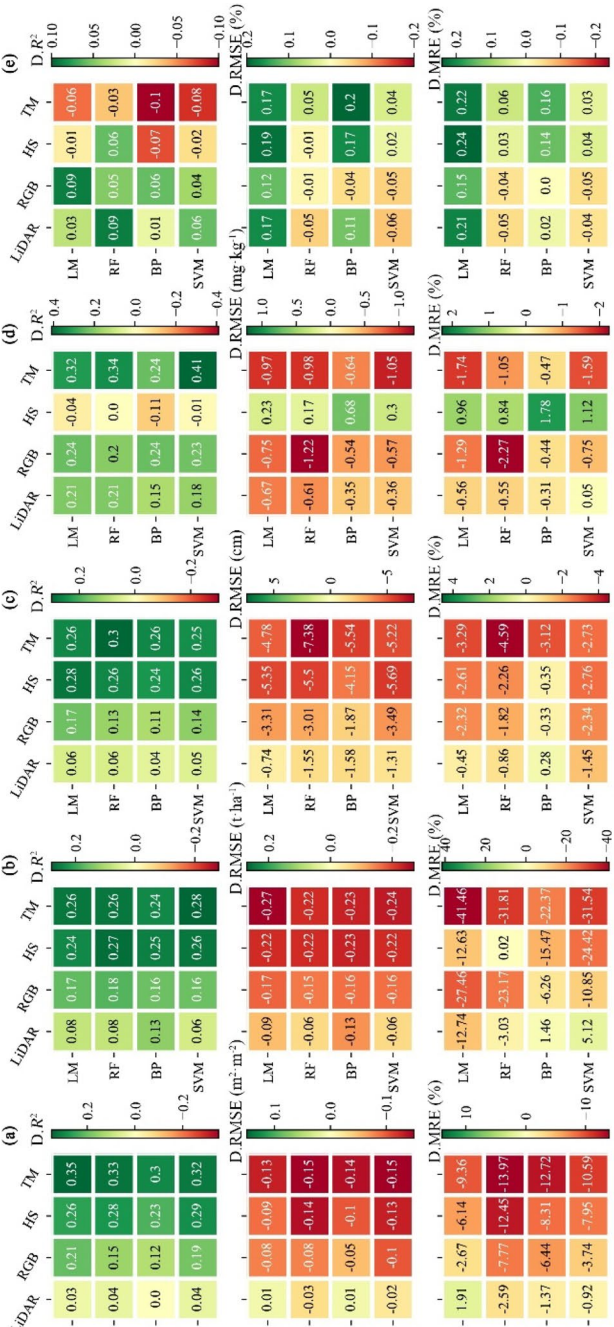

Fig. 11 Comparing the estimation accuracy of maize phenotyping using single-source and multi-source UAV data (D.R^2, D.RMSE, and D.MRE denote R^2, RMSE, and MRE values of differences between multi-source UAV data and single-source UAV data, respectively; e.g., D.$R^2 = R^2$ of multi-source dataset minus R^2 of single-source dataset)

suitable for modeling with large samples, and BP is required to be debugged many times until its performance is optimized with satisfying robustness for determining the optimal parameters; while RF performs well in modeling with small samples (Pham & Brabyn, 2017; Wang et al., 2016). Therefore, SVM and RF outperformed BP in the case of fewer inputs (Mountrakis et al., 2011; Xu et al., 2020). Regarding W estimation, the performance of four methods was moderate, which might be not due to the model itself but the errors contained TM dataset, which was derived from e.g., changeable weather conditions, or the limited irrigation levels applied in plots. The relatively coarse spatial resolution of TM dataset (~ 20 cm) might also hamper its ability to maize phenotyping.

Figure 12 shows the scatters between measured and estimated parameters using the optimal multi-source UAV dataset (determined in "Maize phenotyping using multi-source UAV RS data" section). As expected from the comparable RMSE and R^2, the distribution feature of estimated against measured crop parameters for each algorithm was similar. It is worth noting that all the methods tended to slightly underestimate AGB when it was over 3 t ha^{-1}, whereas the underestimation was not obvious for LAI and CH estimation. This could be because the importance values of HS and RGB variables for AGB estimation were higher than LiDAR variables; while LiDAR variables played a decisive role in LAI and CH estimation. Thus, the saturation issues and surrounding noises contained in the optical dataset degraded AGB estimation accuracy more evidently than LAI and CH estimation. Besides, maize with lower W values was cultivated at plots deficient in nutrient or irrigation, and their temperature was higher than the surroundings. The high temperature of these topical canopies might be easily affected by the changeable weather conditions, which impaired TM-integrated model performance.

This study, like many others, has uncertainties on parameter estimation. Ground measurement uncertainties caused by e.g., the limited size of plots and changeable surrounding environment, could be alleviated via repeating measurement and standard operation.

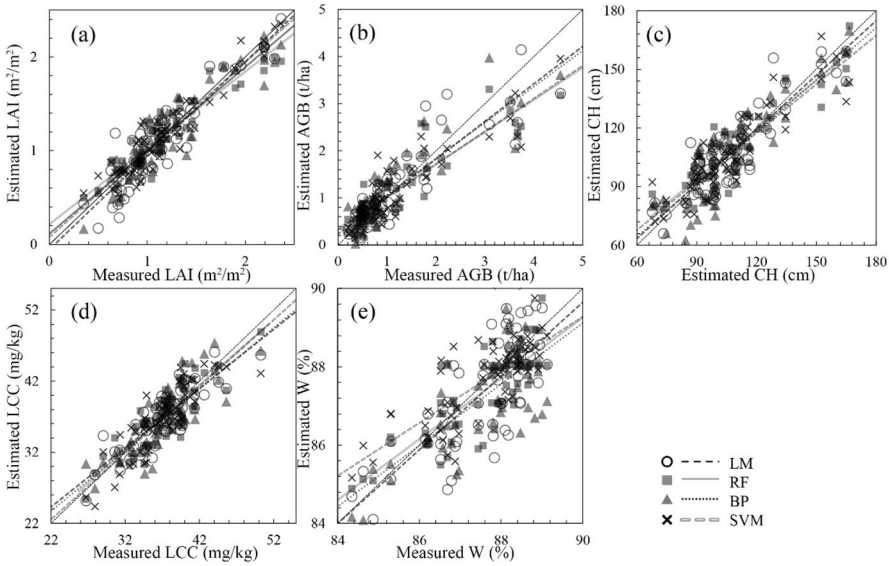

Fig. 12 Scatters of measured and estimated phenotypic parameters of maize: **a** LAI, **b** AGB, **c** CH, **d** LCC, and **e** W using LM, BP, RF, and SVM algorithms

Uncertainties of model structure can be indirectly revealed via the intercomparison of different regression models. In such a context, the comparable estimates of four regression models indicated that our research was reliable. In addition, this study was conducted at the vegetative growth of maize. During this period, the number and area of leaves increased, and organic matter gradually accumulated, thus LAI, AGB, and CH increased with a nearly linear relationship trend. However, during the reproductive growth stage, LAI and CH remained constant, while AGB increased owing to the grain filling process. Therefore, an in-depth study is required to better consider comprehensive factors, such as environmental conditions, plant species, development stages, as well as their interactions on crop phenotyping. Furthermore, the spatial resolutions of multi-source data were different owing to the specification of different sensors, while further studies could eliminate this effect to determine a better UAV agro-monitoring scheme for crop phenotyping.

UAV agro-monitoring scheme designed for precision agriculture

In precision agriculture, the estimation accuracy of crop phenotypic parameters should be considered together with comprehensive factors, such as the costs of UAV sensors, flight risk, and flight speed and coverage. Currently, few studies have applied LiDAR to agronomic applications due to its high costs. As CH in agro-ecosystems is low compared to macrophanerophytes in forest ecosystems, the super penetration ability of LiDAR system may be ineffectively applied in farmland; but LiDAR point clouds can generate raster imageries with pretty high spatial resolutions, which exhibits advantages in revealing subtle differences of homogeneous crop canopies. However, previous studies have demonstrated that SfM point clouds derived from RGB/MS imageries with a high spatial resolution and overlaps can accurately fulfill the requirement of crop phenotyping as well (Zhu et al., 2019a, b).

HS data performed best regarding LCC estimation. However, the high cost (~ $ 50, 000) and weight (> 1 kg) are two undeniable disadvantages. Limited by the battery life, UAV flights, such as a DJI M600 Pro equipped with a Nano-Hyperspec VNIR HS camera, can last about 20 min with a height of 30–50 m, so UAV HS observations fail to cover large-scale farmland (> 1 ha). By contrast, MS cameras are cost-effective and light, and the flight speed and coverage of UAV MS systems are satisfying. For instance, an eBee wing-fixed UAV equipped with a multiSPEC-4C MS camera can fly for 30–45 min per mission, and the coverage area of each flight for eBee UAV systems with a height of 150 m reaches 100–150 ha. For multi-rotor UAV, such as DJI Phantom 4 Pro, the top horizontal flight speed reaches 72 km h^{-1}, and the take-off and landing of these UAV systems are vertical and easy to conduct. However, the limited bands of MS cameras sometimes hamper their applications in agro-monitoring e.g., estimating chlorophyll and carotenoid content of crops. In such a context, MS along with multi-angle observations are recommended to retrieve LCC/CCC in previous studies. Owing to the characteristics of non-Lambert reflectance for objects, multi-angle observations provide more information of crops (Roosjen et al., 2018; Xu et al., 2019a, b), which partly make up the disadvantages of MS cameras. In recent years, some MS manufacturers have begun to support customer-defined settings regarding the selection of spectral channels for cameras (e.g., MS600 manufactured by Yusense Technology Co., Ltd.), which widens the scope of applications for MS cameras. Therefore, customer-defined MS cameras, which are low-cost and portable, are recommended for crop monitoring schemes in precision and sustainable agriculture.

Considering monitoring robustness, UAV observations with multi-sensor might be better than single-sensor, as information provided by multi-sensors are independent and complementary. According to the results of this study, the integration of LiDAR, RGB, and HS datasets performed better regarding the estimation of LAI, AGB, and CH. As MS cameras can be an alternative to LiDAR and HS sensors, considering practical costs, UAV RGB texture/SfM (for structure detection) + customer-defined MS systems (for spectral information) are recommended in agricultural applications, while in-depth research is needed to further validate this conclusion. Moreover, regarding W and LCC estimation, a single-source TM and HS UAV dataset performed best, respectively, and to some extent, the fusion of multi-source UAV data reduced W and LCC estimation accuracy. Therefore, it is necessary to trade off the effects of abundant information and implied errors when applying a multi-source UAV dataset in crop phenotyping.

Conclusion

In this study, field-scale UAV HS, RGB, TM, and LiDAR data along with four regression methods (i.e., LM, RF, BP, and SVM) were used for the estimation of maize phenotypic parameters (i.e., LAI, AGB, CH, LCC, and W), and the performance of single-source and multi-source UAV datasets were intercompared. Major conclusions are given as follows:

(1) For single-source UAV data, the structure information derived from LiDAR and RGB texture data were suitable for LAI, AGB, and CH estimation; HS data exhibited the best performance on LCC estimation; while TM data were appropriate for W estimation;
(2) Multi-source UAV RS datasets yielded slightly better performance on the estimation of LAI, CH, and AGB, whereas single-source TM and HS outperformed multi-source datasets regarding W and LCC estimation, respectively.
(3) Robust multi-source UAV agro-monitoring schemes for LAI, AGB, and CH estimation were LiDAR + RGB + HS, while optical SfM + customer-defined MS were recommended for routine applications in precision agriculture.

This study integrated the temperature, structure, and spectral information derived from multi-source UAV RS technologies to boost the robustness of maize phenotyping, and further designed appropriate UAV agro-monitoring schemes for specific aims. The finding of this study contributes to field-scale crop phenotyping and extends the applications of UAV RS technologies in precision and sustainable agriculture.

Acknowledgements Thanks for UAV flight assistance provided by Mr. Guicang Ma and Mr. Xuezhi Yue, Mr. Qi Liu, Mr. Peng Zhang, and Mr. Chang Tan, et al., and all experimenters in YCES for the assistant of the field experiment.

Author contributions WZ: Data curation, methodology, formal analysis, writing&editing, investigation. ZS: conceptualization, resources, funding acquisition, supervision, project administration. YH: funding acquisition, supervision, resources. TY: editing. JL: resources. KZ: editing and investigation. JZ and BY: resources, supervision. CS: editing. JP: investigation. SL: software. HH: editing. XL: funding and resources.

Funding This work was supported by the Strategic Priority Research Program of the Chinese Academy of Sciences (XDA23050102, XDA19040303), the Chinese Academy of Sciences Key Project (KFZD-SW-113, KJZD-EW-G20), the National Key Research and Development Program of China (2017YFC0503805), and the National Natural Science Foundation of China (31870421, 41771388), Tianjin Intelligent Manufacturing

Project: Technology of Intelligent Networking by Autonomous Control UAVs for Observation and Application (Tianjin-IMP-2), Yellow River Delta Scholars Program (2020–2024).

Declarations

Conflict of interest The authors declare no conflict of interest.

References

Bendig, J., Bolten, A., Bennertz, S., Broscheit, J., Eichfuss, S., & Bareth, G. (2014). Estimating biomass of barley using Crop Surface Models (CSMs) derived from UAV-based RGB imaging. *Remote Sensing, 6*(11), 10395–10412. https://doi.org/10.3390/rs61110395

Bendig, J., Yu, K., Aasen, H., Bolten, A., Bennertz, S., Broscheit, J., et al. (2015). Combining UAV-based plant height from crop surface models, visible, and near infrared vegetation indices for biomass monitoring in barley. *International Journal of Applied Earth Observation and Geoinformation, 39*, 79–87. https://doi.org/10.1016/j.jag.2015.02.012

Berni, J. A. J., Zarco-Tejada, P. J., Suarez, L., & Fereres, E. (2009). Thermal and narrowband multispectral remote sensing for vegetation monitoring from an unmanned aerial vehicle. *IEEE Transactions on Geoscience and Remote Sensing, 47*(3), 722–738. https://doi.org/10.1109/TGRS.2008.2010457

Cai, Y., Guan, K., Lobell, D., Potgieter, A. B., Wang, S., Peng, J., et al. (2019). Integrating satellite and climate data to predict wheat yield in Australia using machine learning approaches. *Agricultural and Forest Meteorology, 274*, 144–159. https://doi.org/10.1016/j.agrformet.2019.03.010

Cao, Y., Li, G. L., Luo, Y. K., Pan, Q., & Zhang, S. Y. (2020). Monitoring of sugar beet growth indicators using wide-dynamic-range vegetation index (WDRVI) derived from UAV multispectral images. *Computers and Electronics in Agriculture, 171*, 105331. https://doi.org/10.1016/j.compag.2020.105331

Chianucci, F., Disperati, L., Guzzi, D., Bianchini, D., Nardino, V., Lastri, C., et al. (2016). Estimation of canopy attributes in beech forests using true colour digital images from a small fixed-wing UAV. *International Journal of Applied Earth Observation and Geoinformation, 47*, 60–68. https://doi.org/10.1016/j.jag.2015.12.005

Córcoles, J. I., Ortega, J. F., Hernández, D., & Moreno, M. A. (2013). Estimation of leaf area index in onion (*Allium cepa* L.) using an unmanned aerial vehicle. *Biosystems Engineering, 115*(1), 31–42. https://doi.org/10.1016/j.biosystemseng.2013.02.002

Croft, H., Chen, J. M., Wang, R., Mo, G., Luo, S., Luo, X., et al. (2020). The global distribution of leaf chlorophyll content. *Remote Sensing of Environment, 236*, 111479. https://doi.org/10.1016/j.rse.2019.111479

Daughtry, C. S. T., Walthall, C. L., Kim, M. S., de Colstoun, E. B., & McMurtrey, J. E. (2000). Estimating corn leaf chlorophyll concentration from leaf and canopy reflectance. *Remote Sensing of Environment, 74*(2), 229–239. https://doi.org/10.1016/S0034-4257(00)00113-9

de Almeida, C. T., Galvão, L. S., Aragão, L. E., Ometto, J. P. H. B., Jacon, A. D., de SouzaPereira, F. R., et al. (2019). Combining LiDAR and hyperspectral data for aboveground biomass modeling in the Brazilian Amazon using different regression algorithms. *Remote Sensing of Environment, 232*, 111323. https://doi.org/10.1016/j.rse.2019.111323

Dong, T., Liu, J., Shang, J., Qian, B., Ma, B., Kovacs, J. M., et al. (2019). Assessment of red-edge vegetation indices for crop leaf area index estimation. *Remote Sensing of Environment, 222*, 133–143. https://doi.org/10.1016/j.rse.2018.12.032

Duan, S., Li, Z., Wu, H., Tang, B., Ma, L., Zhao, E., & Li, C. (2014). Inversion of the PROSAIL model to estimate leaf area index of maize, potato, and sunflower fields from unmanned aerial vehicle hyperspectral data. *International Journal of Applied Earth Observation and Geoinformation, 26*, 12–20. https://doi.org/10.1016/j.jag.2013.05.007

Feng, A., Zhou, J., Vories, E. D., Sudduth, K. A., & Zhang, M. (2020). Yield estimation in cotton using UAV-based multi-sensor imagery. *Biosystems Engineering, 193*, 101–114. https://doi.org/10.1016/j.biosystemseng.2020.02.014

Gnyp, M. L., Bareth, G., Li, F., Lenz-Wiedemann, V. I. S., Koppe, W., Miao, Y., et al. (2014). Development and implementation of a multiscale biomass model using hyperspectral vegetation indices for winter wheat in the North China Plain. *International Journal of Applied Earth Observation and Geoinformation, 33*, 232–242. https://doi.org/10.1016/j.jag.2014.05.006

González-Jaramillo, V., Fries, A., & Bendix, J. (2019). AGB estimation in a Tropical Mountain Forest (TMF) by means of RGB and multispectral images using an Unmanned Aerial Vehicle (UAV). *Remote Sensing, 11*(12), 1413. https://doi.org/10.3390/rs11121413

Haboudane, D., Miller, J. R., Tremblay, N., Zarco-Tejada, P. J., & Dextraze, L. (2002). Integrated narrow-band vegetation indices for prediction of crop chlorophyll content for application to precision agriculture. *Remote Sensing of Environment, 81*(2), 416–426. https://doi.org/10.1016/S0034-4257(02)00018-4

Hunt, E. R., Horneck, D. A., Spinelli, C. B., Turner, R. W., Bruce, A. E., Gadler, D. J., et al. (2018). Monitoring nitrogen status of potatoes using small unmanned aerial vehicles. *Precision Agriculture, 19*(2), 314–333. https://doi.org/10.1007/s11119-017-9518-5

Jay, S., Baret, F., Dutartre, D., Malatesta, G., Héno, S., Comar, A., et al. (2018). Exploiting the centimeter resolution of UAV multispectral imagery to improve remote-sensing estimates of canopy structure and biochemistry in sugar beet crops. *Remote Sensing of Environment*. https://doi.org/10.1016/j.rse.2018.09.011

Jay, S., Maupas, F., Bendoula, R., & Gorretta, N. (2017). Retrieving LAI, chlorophyll and nitrogen contents in sugar beet crops from multi-angular optical remote sensing: Comparison of vegetation indices and PROSAIL inversion for field phenotyping. *Field Crops Research, 210*, 33–46. https://doi.org/10.1016/j.fcr.2017.05.005

Kanning, M., Kühling, I., Trautz, D., & Jarmer, T. (2018). High-resolution UAV-based hyperspectral imagery for LAI and chlorophyll estimations from wheat for yield prediction. *Remote Sensing, 10*(12), 2000. https://doi.org/10.3390/rs10122000

Karpina, M., Jarząbek-Rychard, M., Tymków, P., & Borkowski, A. (2016). UAV-based automatic tree growth measurement for biomass estimation. *ISPRS—International Archives of the Photogrammetry Remote Sensing and Spatial Information Sciences, 8*, 685–688. https://doi.org/10.5194/isprsarchives-XLI-B8-685-2016

Kullberg, E. G., DeJonge, K. C., & Chávez, J. L. (2017). Evaluation of thermal remote sensing indices to estimate crop evapotranspiration coefficients. *Agricultural Water Management, 179*, 64–73. https://doi.org/10.1016/j.agwat.2016.07.007

Lei, F., Crow, W. T., Kustas, W. P., Dong, J., Yang, Y., Knipper, K. R., et al. (2020). Data assimilation of high-resolution thermal and radar remote sensing retrievals for soil moisture monitoring in a drip-irrigated vineyard. *Remote Sensing of Environment, 239*, 111622. https://doi.org/10.1016/j.rse.2019.111622

Li, W., Niu, Z., Chen, H., Li, D., Wu, M., & Zhao, W. (2016). Remote estimation of canopy height and aboveground biomass of maize using high-resolution stereo images from a low-cost unmanned aerial vehicle system. *Ecological Indicators, 67*, 637–648. https://doi.org/10.1016/j.ecolind.2016.03.036

Li, Z., Li, Z., Fairbairn, D., Li, N., Xu, B., Feng, H., & Yang, G. (2019). Multi-LUTs method for canopy nitrogen density estimation in winter wheat by field and UAV hyperspectral. *Computers and Electronics in Agriculture, 162*, 174–182. https://doi.org/10.1016/j.compag.2019.04.005

Luo, S., Wang, C., Xi, X., Nie, S., Fan, X., Chen, H., et al. (2019). Combining hyperspectral imagery and LiDAR pseudo-waveform for predicting crop LAI, canopy height and above-ground biomass. *Ecological Indicators, 102*, 801–812. https://doi.org/10.1016/j.ecolind.2019.03.011

Maes, W. H., & Steppe, K. (2012). Estimating evapotranspiration and drought stress with ground-based thermal remote sensing in agriculture: A review. *Journal of Experimental Botany, 63*, 4671–4712. https://doi.org/10.1093/jxb/ers165

Maimaitijiang, M., Sagan, V., Sidike, P., Hartling, S., Esposito, F., & Fritschi, F. B. (2020). Soybean yield prediction from UAV using multimodal data fusion and deep learning. *Remote Sensing of Environment, 237*, 111599. https://doi.org/10.1016/j.rse.2019.111599

Mountrakis, G., Im, J., & Ogole, C. (2011). Support vector machines in remote sensing: A review. *ISPRS Journal of Photogrammetry and Remote Sensing, 66*(3), 247–259. https://doi.org/10.1016/j.isprsjprs.2010.11.001

Niu, Y., Zhang, L., Zhang, H., Han, W., & Peng, X. (2019). Estimating above-ground biomass of maize using features derived from UAV-based RGB imagery. *Remote Sensing, 11*(11), 1261. https://doi.org/10.3390/rs11111261

Pablo Rivera-Caicedo, J., Verrelst, J., Munoz-Mari, J., Camps-Valls, G., & Moreno, J. (2017). Hyperspectral dimensionality reduction for biophysical variable statistical retrieval. *Isprs Journal of Photogrammetry and Remote Sensing, 132*, 88–101. https://doi.org/10.1016/j.isprsjprs.2017.08.012

Peng, Y., Nguy-Robertson, A., Arkebauer, T., & Gitelson, A. (2017). Assessment of canopy chlorophyll content retrieval in maize and soybean: Implications of hysteresis on the development of generic algorithms. *Remote Sensing, 9*(3), 226. https://doi.org/10.3390/rs9030226

Pham, L. T. H., & Brabyn, L. (2017). Monitoring mangrove biomass change in Vietnam using SPOT images and an object-based approach combined with machine learning algorithms. *ISPRS Journal of Photogrammetry and Remote Sensing, 128*, 86–97. https://doi.org/10.1016/j.isprsjprs.2017.03.013

Roosjen, P. P. J., Brede, B., Suomalainen, J. M., Bartholomeus, H. M., Kooistra, L., & Clevers, J. G. P. W. (2018). Improved estimation of leaf area index and leaf chlorophyll content of a potato crop using multi-angle spectral data—potential of unmanned aerial vehicle imagery. *International Journal of Applied Earth Observation and Geoinformation, 66*, 14–26. https://doi.org/10.1016/j.jag.2017.10.012

Roth, L., Aasen, H., Walter, A., & Liebisch, F. (2018). Extracting leaf area index using viewing geometry effects—A new perspective on high-resolution unmanned aerial system photography. *ISPRS Journal of Photogrammetry and Remote Sensing, 141*, 161–175. https://doi.org/10.1016/j.isprsjprs.2018.04.012

Schneider, F. D., Kukenbrink, D., Schaepman, M. E., Schimel, D. S., & Morsdorf, F. (2019). Quantifying 3D structure and occlusion in dense tropical and temperate forests using close-range LiDAR. *Agricultural and Forest Meteorology, 268*, 249–257. https://doi.org/10.1016/j.agrformet.2019.01.033

Su, W., Zhang, M., Bian, D., Liu, Z., Huang, J., Wang, W., et al. (2019). Phenotyping of corn plants using Unmanned Aerial Vehicle (UAV) images. *Remote Sensing, 11*(17), 2021. https://doi.org/10.3390/rs11172021

Széles, A. V., Megyes, A., & Nagy, J. (2012). Irrigation and nitrogen effects on the leaf chlorophyll content and grain yield of maize in different crop years. *Agricultural Water Management, 107*, 133–144. https://doi.org/10.1016/j.agwat.2012.02.001

Taghvacian, S., Chavez, J. L., & Hansen, N. C. (2012). Infrared thermometry to estimate crop water stress index and water use of irrigated maize in Northeastern Colorado. *Remote Sensing, 4*(11), 3619–3637. https://doi.org/10.3390/rs4113619

Verrelst, J., Pablo Rivera, J., Veroustraete, F., Munoz-Mari, J., Clevers, J. G. P. W., Camps-Valls, G., & Moreno, J. (2015). Experimental Sentinel-2 LAI estimation using parametric, non-parametric and physical retrieval methods—A comparison. *ISPRS Journal of Photogrammetry and Remote Sensing, 108*, 260–272. https://doi.org/10.1016/j.isprsjprs.2015.04.013

Wang, L., Zhou, X., Zhu, X., Dong, Z., & Guo, W. (2016). Estimation of biomass in wheat using random forest regression algorithm and remote sensing data. *The Crop Journal, 4*(3), 212–219. https://doi.org/10.1016/j.cj.2016.01.008

Wang, S., Garcia, M., Bauer-Gottwein, P., Jakobsen, J., Zarco-Tejada, P. J., Bandini, F., et al. (2019a). High spatial resolution monitoring land surface energy, water and CO_2 fluxes from an Unmanned Aerial System. *Remote Sensing of Environment, 229*, 14–31. https://doi.org/10.1016/j.rse.2019.03.040

Wang, Y., Zhang, K., Tang, C., Cao, Q., Tian, Y., Zhu, Y., et al. (2019b). Estimation of rice growth parameters based on linear mixed-effect model using multispectral images from fixed-wing unmanned aerial vehicles. *Remote Sensing, 11*(11), 1371. https://doi.org/10.3390/rs11111371

Weiss, M., Jacob, F., & Duveiller, G. (2020). Remote sensing for agricultural applications: A meta-review. *Remote Sensing of Environment, 236*, 111402. https://doi.org/10.1016/j.rse.2019.111402

Xie, Q., Dash, J., Huete, A., Jiang, A., Yin, G., Ding, Y., et al. (2019). Retrieval of crop biophysical parameters from Sentinel-2 remote sensing imagery. *International Journal of Applied Earth Observation and Geoinformation, 80*, 187–195. https://doi.org/10.1016/j.jag.2019.04.019

Xu, K., Su, Y., Liu, J., Hu, T., Jin, S., Ma, Q., et al. (2020). Estimation of degraded grassland aboveground biomass using machine learning methods from terrestrial laser scanning data. *Ecological Indicators, 108*, 105747. https://doi.org/10.1016/j.ecolind.2019.105747

Xu, M., Liu, R., Chen, J. M., Liu, Y., Shang, R., Ju, W., et al. (2019a). Retrieving leaf chlorophyll content using a matrix-based vegetation index combination approach. *Remote Sensing of Environment, 224*, 60–73. https://doi.org/10.1016/j.rse.2019.01.039

Xu, X. Q., Lu, J. S., Zhang, N., Yang, T. C., He, J. Y., Yao, X., et al. (2019b). Inversion of rice canopy chlorophyll content and leaf area index based on coupling of radiative transfer and Bayesian network models. *ISPRS Journal of Photogrammetry and Remote Sensing, 150*, 185–196. https://doi.org/10.1016/j.isprsjprs.2019.02.013

Yang, G., Liu, J., Zhao, C., Li, Z., Huang, Y., Yu, H., et al. (2017). Unmanned aerial vehicle remote sensing for field-based crop phenotyping: current status and perspectives. *Frontiers in Plant Science, 8*, 1111. https://doi.org/10.3389/fpls.2017.01111

Yao, X., Wang, N., Liu, Y., Cheng, T., Tian, Y., Chen, Q., & Zhu, Y. (2017). Estimation of wheat LAI at middle to high levels using unmanned aerial vehicle narrowband multispectral imagery. *Remote Sensing, 9*(12), 1304. https://doi.org/10.3390/rs9121304

Ye, N., van Leeuwen, L., & Nyktas, P. (2020). Estimating aboveground biomass of the mangrove forests on northeast Hainan Island in China using an upscaling method from field plots, UAV-LiDAR data and Sentinel-2 imagery. *International Journal of Applied Earth Observation and Geoinformation, 85*, 101986. https://doi.org/10.1016/j.jag.2019.101986

Yu, K., Lenz-Wiedemann, V., Chen, X., & Bareth, G. (2014). Estimating leaf chlorophyll of barley at different growth stages using spectral indices to reduce soil background and canopy structure effects. *ISPRS Journal of Photogrammetry and Remote Sensing, 97*, 58–77. https://doi.org/10.1016/j.isprsjprs.2014.08.005

Ye, N., van Leeuwen, L., & Nyktas, P. (2019). Analysing the potential of UAV point cloud as input in quantitative structure modelling for assessment of woody biomass of single trees. *International Journal of Applied Earth Observation and Geoinformation, 81*, 47–57. https://doi.org/10.1016/j.jag.2019.05.010

Yue, J., Feng, H., Jin, X., Yuan, H., Li, Z., Zhou, C., et al. (2018). A Comparison of crop parameters estimation using images from UAV-mounted snapshot hyperspectral sensor and high-definition digital camera. *Remote Sensing, 10*(7), 1138. https://doi.org/10.3390/rs10071138

Yue, J., Yang, G., Li, C., Li, Z., Wang, Y., Feng, H., & Xu, B. (2017). Estimation of winter wheat aboveground biomass using unmanned aerial vehicle-based snapshot hyperspectral sensor and crop height improved models. *Remote Sensing, 9*(7), 708. https://doi.org/10.3390/rs9070708

Zhou, X., Zheng, H. B., Xu, X. Q., He, J. Y., Ge, X. K., Yao, X., et al. (2017). Predicting grain yield in rice using multi-temporal vegetation indices from UAV-based multispectral and digital imagery. *ISPRS Journal of Photogrammetry and Remote Sensing, 130*, 246–255. https://doi.org/10.1016/j.isprsjprs.2017.05.003

Zhu, W., Sun, Z., Huang, Y., Lai, J., Li, J., Zhang, J., et al. (2019a). Improving field-scale wheat LAI retrieval based on UAV remote-sensing observations and optimized VI-LUTs. *Remote Sensing, 11*(20), 2456. https://doi.org/10.3390/rs11202456

Zhu, W., Sun, Z., Peng, J., Huang, Y., Li, J., Zhang, J., et al. (2019b). Estimating maize above-ground biomass using 3D point clouds of multi-source unmanned aerial vehicle data at multi-spatial scales. *Remote Sensing, 11*(22), 2678. https://doi.org/10.3390/rs11222678

Zhu, W., Sun, Z., Yang, T., Li, J., Peng, J., Zhu, K., et al. (2020). Estimating leaf chlorophyll content of crops via optimal unmanned aerial T vehicle hyperspectral data at multi-scales. *Computers and Electronics in Agriculture, 178*, 105786. https://doi.org/10.1016/j.compag.2020.105786

Authors and Affiliations

Wanxue Zhu[1,2] · Zhigang Sun[1,2,3,4] · Yaohuan Huang[2,5] · Ting Yang[4] · Jing Li[1] · Kangying Zhu[1,2] · Junqiang Zhang[6,7] · Bin Yang[7] · Changxiu Shao[1] · Jinbang Peng[1,2] · Shiji Li[1,2] · Hualang Hu[8] · Xiaohan Liao[2,5,9,10]

1 Key Laboratory of Ecosystem Network Observation and Modeling, Institute of Geographic Sciences and Natural Resources Research, Chinese Academy of Sciences, Beijing 100101, China

2 College of Resources and Environment, University of Chinese Academy of Sciences, Beijing 100049, China

3 Shandong Dongying Institute of Geographic Sciences, Dongying 257000, China

4 CAS Engineering Laboratory for Yellow River Delta Modern Agriculture, Institute of Geographic Sciences and Natural Resources Research, Chinese Academy of Sciences, Beijing 100101, China

5 State Key Laboratory of Resources and Environmental Information System, Institute of Geographic Sciences and Natural Resources Research, Chinese Academy of Sciences, Beijing 100101, China

6 Fine Mechanics and Physics, Changchun Institute of Optics, Chinese Academy of Sciences, Changchun 130033, China

7 Yusense Information Technology and Equipment (Qingdao) Ltd., Qingdao 266000, China

8 Key Laboratory of Cultivated Land Use/Ministry of Agriculture and Rural Affairs, Academy of Agricultural Planning and Engineering, Beijing 100125, China

[9] Research Center for UAV Applications and Regulation, Chinese Academy of Science, Beijing 100101, China

[10] Institute of UAV Application Research, Tianjin and CAS, Tianjin 301800, China